

## The 10 pc Neighborhood of Habitable Zone Exoplanetary Systems: Threat Assessment from Stellar Encounters & Supernovae

TISYAGUPTA PYNE,<sup>1,2</sup> RAVINDER K. BANYAL <sup>1</sup>, C. SWASTIK <sup>3,1,4</sup> AND AYANABHA DE <sup>1</sup>

<sup>1</sup>*Indian Institute of Astrophysics, Koramangala 2nd Block, Bangalore 560034, India*

<sup>2</sup>*Integrated Science Education and Research Centre, Visva-Bharati University, Santiniketan, 731235, India*

<sup>3</sup>*Dipartimento di Fisica, Università degli Studi di Milano, Via Celoria 16, 20133 Milano, Italy*

<sup>4</sup>*Pondicherry University, R.V. Nagar, Kalapet, 605014, Puducherry, India*

(Accepted November 4, 2024)

Submitted to AJ

### Abstract

The habitability of a planet is influenced by both its parent star and the properties of its local stellar neighborhood. Potential threats to habitability from the local stellar environment mainly arise from two factors: cataclysmic events such as powerful stellar explosions and orbital perturbations induced by close stellar encounters. Among the 4,500+ exoplanet-hosting stars, about 140+ are known to host planets in their habitable zones. In this study, we use *Gaia DR3* data to investigate the 10 pc stellar neighborhood of the 84 habitable zone systems (HZS) closest to the Sun. We assess the possible risks that local stellar environment of these HZS pose to their habitability. In particular, we find that HD 165155 has a high stellar density around it, making it likely to experience at least one flyby encounter within a span of 5 Gyr. We also identified two high-mass stars ( $M \geq 8M_{\odot}$ ) as potential progenitors of supernovae, which could threaten the long-term survivability of habitable zone systems HD 48265 and TOI-1227. Further, to quantify the similarity between habitable zone stars and the Sun, as well as their respective 10 pc stellar environments, we employ various astrophysical parameters to define a Solar Similarity Index (SSI) and a Neighborhood Similarity Index (NSI). Our analysis suggests that HD 40307 exhibits the closest resemblance to the solar system, while HD 165155 shows the least resemblance.

**Keywords:** Exoplanet astronomy(486), Habitable zone(696), Habitable planets(695), Solar neighborhood(1509), Gaia(2360), Close encounters(255)

### 1. INTRODUCTION

Finding a habitable world is one of the primary goals of exoplanetary research. The study of habitability is a rapidly growing field in exoplanet science, with over 150 confirmed discoveries of planets residing in the habitable zones' of stars already made (Fujii et al. 2018; Schwieterman et al. 2018; Glaser et al. 2020; Lisse et al. 2020; Hill et al. 2023). Traditionally, the habitable zone (HZ) is defined as the annular region around a star where liquid

water can exist on a planet under sufficient atmospheric pressure.

In modern lexicon, habitable zones are typically categorized into two broad types (Kasting et al. 1993; Underwood et al. 2003). The first is the conservative habitable zone, which is defined by an inner boundary where the intense radiant energy from the star may induce a runaway greenhouse effect, resulting in the vaporization of surface water. Its outer boundary is determined by the distance from the central star at which a planet's cloud-free CO<sub>2</sub> atmosphere can maintain a surface temperature of 273 K. In contrast, the second type, known as the optimistic habitable zone (OHZ), encompasses regions receiving radiation levels ranging between those experi-

enced by Mars  $\sim 4$  billion years ago and Venus around 1 billion year ago. (Kopparapu et al. 2013, 2014; Ware et al. 2022).

In the galactic context, the conditions favourable for life are also dependent on spatial and temporal location of star-planet systems within the Milky Way (Gonzalez et al. 2001; Lineweaver et al. 2004). Aspects of galactic habitability include the radiation threat from high-energy events like Supernovae (SNe), Gamma-ray bursts (GRBs), presence of heavy elements that are crucial for the formation of rocky planets, star-forming regions and epoch of planet formation in the galaxy (Spitoni et al. 2017; Spinelli et al. 2021; Swastik et al. 2022; Spinelli & Ghirlanda 2023; Swastik et al. 2024).

While the concept of HZ is vital in the search for habitable worlds, the stellar environment of the planet also plays an important role in determining longevity and maintenance of habitability. In particular, a planet’s habitability can be greatly influenced by the type and distribution of stars surrounding the exoplanet hosting star. Studies have shown that a high rate of catastrophic events, such as supernovae and close stellar encounters in regions of high stellar density, is not conducive to the evolution of complex life forms and the maintenance of habitability over long periods (Jiménez-Torres et al. 2013; Spitoni et al. 2017; Spinelli et al. 2021; Spinelli & Ghirlanda 2023). Important as they are, these theoretical ideas have not been tested against the observed ensemble of extrasolar planets.

The growing number of exoplanet discoveries has enabled researchers to gather robust statistics, warranting further investigation into their stellar environments (Narang et al. 2018; Swastik et al. 2021; Unni et al. 2022; Narang et al. 2023; Banerjee et al. 2024). The latest census of confirmed exoplanetary systems and their astrophysical properties are available at various public archives (Schneider et al. 2011; Akeson et al. 2013; Han et al. 2014; NASA Exoplanet Science Institute 2020). Out of the 5500+ discovered exoplanets so far, 146 stars are known to host 158 rocky and gaseous planets within their HZ, as documented in the Catalog of Habitable Zone Exoplanets (Kane & Gelino 2012; Hill et al. 2023). Some of these systems are potential targets for detailed atmospheric characterization and the detection of bio-signatures in current and future missions (Stark et al. 2014; Tinetti et al. 2018; Redfield et al. 2024).

In this work, we focus on the local stellar environment of stars hosting habitable zone exoplanets. More specifically, we use *Gaia DR3* archive to analyze the 10 pc neighborhood (stars within a sphere of 10 pc radius) surrounding the known habitable zone systems (HZS). This involves extracting sources from the *Gaia DR3*

archive with measured parallaxes from  $\varpi \approx 750$  mas to  $\varpi \approx 4.5$  mas which correspond to the nearest (Proxima Centauri) and the farthest (Kepler-296) HZS. The rationale for selecting a 10 pc region is based on studies indicating that if a star within this range evolves into a Type-Ia/Ibc SNe, it would produce X-rays and  $\gamma$ -rays with sufficient fluence (total energy emitted by a SNe per unit area) to significantly disrupt a planet’s ozone layer (Spinelli & Ghirlanda 2023). Additionally, the 10 pc neighborhood of the solar system, well-studied using *Gaia DR3* by Reylé et al. (2021), provides a valuable reference for exoplanet demographic comparison. We further explore the likelihood of stellar encounters and supernovae that could pose a threat to the habitability of these systems. We also compare the 10 pc neighborhood of these HZS with the 10 pc solar neighborhood sample compiled by Reylé et al. (2021) and Reylé et al. (2022).

We define the Solar Similarity Index (SSI) as a metric for comparing the properties of the habitable zone planet-hosting stars with those of the Sun. Similarly, the Neighborhood Similarity Index (NSI) is a metric used to compare the properties and distribution of objects within their respective volumes of 10 pc radius. These indices are then used to determine which habitable systems have the closest resemblance to our solar system and its 10 pc environment. The closer the index is to 1, the more similar it is. The stellar and planetary data (see Table 1) for this study are obtained from the *Gaia DR3* and the NASA Exoplanet Archive (NEA) (Gaia Collaboration et al. 2023a; Akeson et al. 2013; NASA Exoplanet Science Institute 2020).

From here on, the paper is organized as follows: In Section 2, we describe our primary sample of HZS and the construction of their 10 pc neighborhoods. In Section 3, we discuss the influence of the stellar neighborhoods on habitability and present our main results. In Section 4, we address the incompleteness of *Gaia* data and its implications for our findings. Finally, in Section 5 we summarize and conclude this work.

## 2. SAMPLE SELECTION

In this section, we describe the process of our sample selection which mainly consists of two parts. The first part involves selecting 146 planet-hosting stars from the Habitable Zone Gallery<sup>1</sup>, which constitutes our *primary sample* of HZS. For the second part, we used the *Gaia DR3* catalog to select stars within the 10 pc neighbor-

<sup>1</sup> <https://hzgallery.org/>

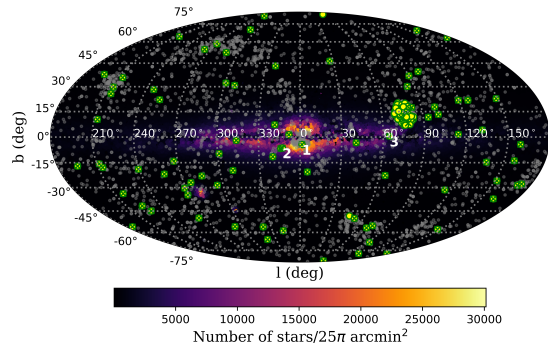


**Figure 1.** Sky positions of exoplanet-hosting stars projected on Mollweide map. HZS are denoted by yellow-green circles, while the remaining population of exoplanets is represented by gray circles. The studied sample of 84 HZS, located within 220 pc of the Sun, is represented by crossed yellow-green circles. The three high-density HZS located near the galactic plane are labeled 1, 2 and 3 in white. The colorbar represents the stellar density, i.e., the number of stars having  $G \geq 15$  within a radius of 5 arcmin.

hood of 144 HZ host stars<sup>2</sup>. The subset of stars in each 10 pc HZ neighborhood was curated from a larger 25 pc dataset, as explained in Section 2.2.

### 2.1. Habitable Zone Gallery

The Habitable Zone Gallery is an online catalog of known exoplanets and their orbital parameters (Kane & Gelino 2012; Hill et al. 2023), constructed using information from larger databases such as Exoplanet Data Explorer<sup>3</sup> and the NEA<sup>4</sup>. The Gallery demarcates the habitable zones of each planet-hosting star as defined by Kopparapu et al. (2013, 2014). It also calculates the fraction of time a planet spends in the habitable zone, which can vary from 0% to 100% depending on the planet’s eccentricity and orbital distance. This catalog is regularly updated and it serves as a valuable resource for researchers studying the habitability of exoplanets.

Our primary sample of HZS, drawn from the Habitable Zone Gallery, comprises 146 systems hosting 158 planets whose orbits fully reside within the optimistic habitable zone of their host stars. Of these 158 planets, 35 are presumably rocky planets ( $\leq 2R_{\oplus}$ ), 122 are gaseous planets, and 1 has an undetermined mass and radius. While the giant planets themselves are inhospitable, they may host rocky exomoons orbiting them under favorable conditions for life (Heller 2012; Heller

& Barnes 2013). Additionally, the moons of giant planets located at the outer edge of the habitable zone could generate sufficient energy through tidal heating (Heller & Barnes 2013; Heller & Armstrong 2014; Hill et al. 2018; Hill et al. 2023). The astrophysical parameters of these systems were obtained from the NASA Exoplanet Archive. Figure 1 shows the all-sky distribution of exoplanet hosting stars in a Mollweide projection. The nearest HZS to the Sun is Proxima Centauri, located at a distance of 1.3 pc, while the farthest is Kepler-1636, at a distance of 2.2 kpc.

### 2.2. Curating the 10 pc neighborhood

For studying the 10 pc environment of HZS using *Gaia* DR3, we have to contend with two major issues:

- The ambiguity of stars belonging to the 10 pc region due to distance and magnitude dependent parallax errors (see Appendix B), and
- The incompleteness of *Gaia* data, i.e., *Gaia*’s inability to detect sources outside  $21 \lesssim G \lesssim 3$  magnitude range and additional cuts on various astrophysical parameters, impacting its overall dataset (Reylé et al. 2021; Gaia Collaboration et al. 2023a).

The relative parallax errors in *Gaia* data can significantly affect distance estimates and introduce ambiguity in defining the 10 pc boundary. This means that a strict 10 pc neighborhood sample returned by a *Gaia* query (see Figure 2) may include some stars with large parallax errors that could, in reality, be outside the 10 pc sphere, or it may exclude stars that are truly within the 10 pc boundary. Therefore, to address this issue, the 10 pc stellar environment for each HZ system was constructed from a superset of neighboring stars distributed within a sphere of radius 25 pc. For this, we used a simple bootstrapping approach that alleviates the need to define an exact 10 pc boundary and helps constrain the uncertainties of astrophysical parameters of neighborhood stars at the ensemble level, which we later use for quantifying the similarity indices.

Apart from the stated ambiguity in the star count within the 10 pc sample, Figure 2 shows a decline in the number of neighborhood stars around HZS beyond a distance of  $\sim 300$  pc. This selection bias (under count) arises due to the incompleteness of *Gaia* data, which is discussed later in Section 4. Figure 3 shows how the relative parallax error of *Gaia* detected stars increases with decreasing parallax (i.e., with increasing distance from Sun). Since our goal is to study the 10 pc region around HZ stars, if the distance error were to exceed 10 pc, defining the neighborhood would become arbitrary. For

<sup>2</sup> Parallax measurements were not available for two of the systems, Kepler-1652 and Kepler-1410.

<sup>3</sup> <http://exoplanets.org/table>

<sup>4</sup> <https://exoplanetarchive.ipac.caltech.edu/>

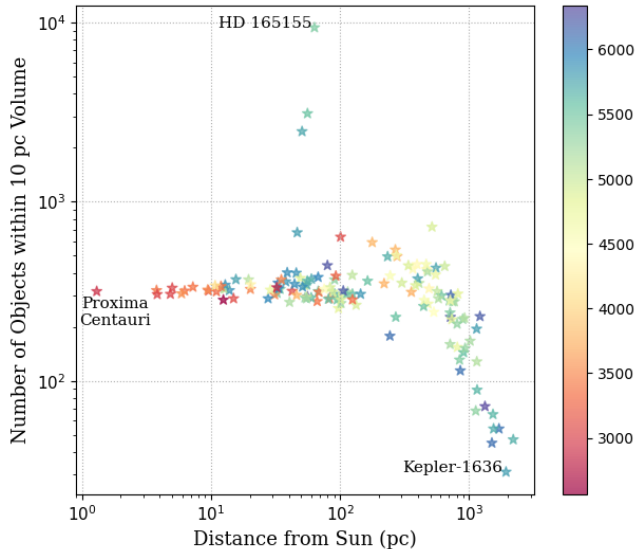


**Figure 2.** The 10 pc neighborhood star count for 144 HZS and their distance from the Sun. The colorbar represents the effective temperature  $T_{\text{eff}}$  (K) of HZ stars.

the *Gaia* detected stars shown in Figure 3, the relative parallax error exceeds 5% beyond 220 pc ( $\varpi \approx 4.5$  mas) which corresponds to a distance error  $\sim 10$  pc. Hence, we only consider 84 HZS from our primary sample of 146 HZS, which are within a distance of 220 pc from the Sun. By limiting our sample to 220 pc, we also ensure a nearly complete detection of objects within their 10 pc neighborhood, including the cool-dwarfs down to spectral type M6, by *Gaia* (see Section 4).

To curate a 10 pc sample, we begin by issuing a standard ADQL query on the *Gaia DR3* catalog to select stars within 25 pc of a HZS. The query returns all stars around a HZS with distances  $\leq 25$  pc and their astrophysical parameters (see Appendix A). Next, for each HZS, we generate 100,000 random realizations of 10 pc neighborhood stars from this superset by using the bootstrapping method described in Appendix B. The astrophysical parameters<sup>5</sup> and their associated uncertainties are inferred from the sampling distribution of the bootstrap. In Figure 4, we compare the average star count obtained from the bootstrap method and the star count obtained directly from *Gaia*'s 10 pc query for 84 HZS. Apart from a few outliers, the differences are not significant. However, the bootstrap method provides more reliable estimates of the astrophysical parameters of neighborhood stars.

<sup>5</sup> See Table 1 for the astrophysical parameters obtained from the statistical inferences of sampling distributions.

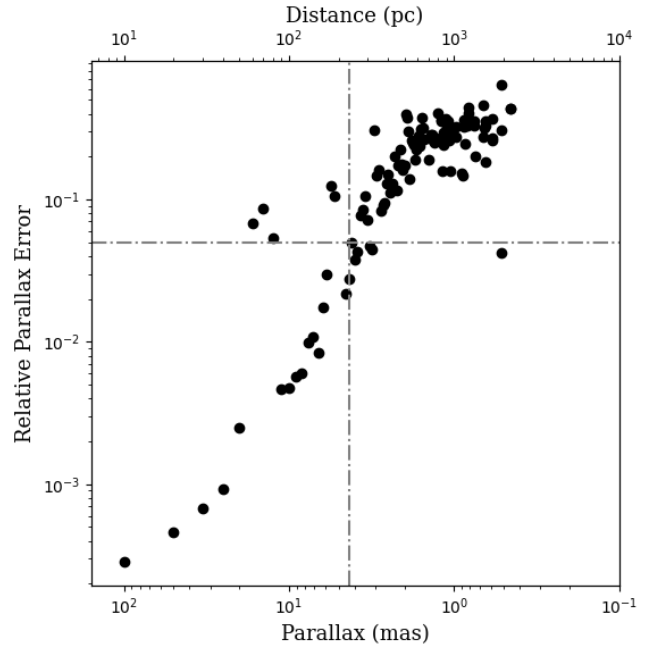


**Figure 3.** Relative parallax errors of *Gaia* detected stars binned at 10 pc intervals as a function of increasing distance from the solar system.

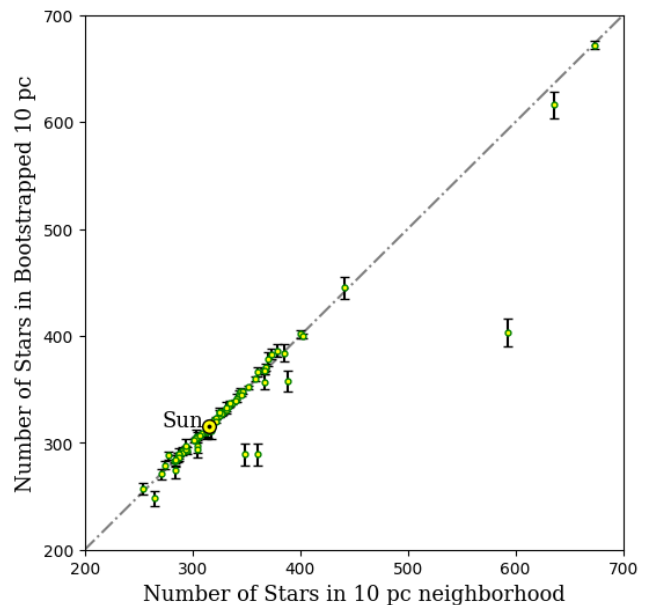


**Figure 4.** Comparison of number of stars returned by *Gaia* ADQL Query. (x-axis) within 10 pc neighborhoods and the 10 pc mean count of stars (y-axis) obtained after  $10^5$  bootstrap runs on a larger dataset of stars within 25 pc region. The errorbars represent  $\pm 1\sigma$  uncertainty in the count of stars after bootstrapping. For brevity, the plot is curtailed at 700 star count, excluding three sources with more than 2000 stars.

Finally, the total star count within the 10 pc region surrounding the 84 HZS is found to be  $\sim 36,000$  stars. This dataset does not include the brighter stars due to the lower magnitude limit ( $G \sim 3$ ) of Gaia. Finding the bright stars in the vicinity of HZS is crucial for assessing the threat to habitability from supernovae. Therefore, to further complement the 10 pc dataset we separately searched the Hipparcos<sup>6</sup> Catalog (Perryman et al. 1997; van Leeuwen 2007), for bright stars. We found 34 bright stars with `hip_mag`  $< 3$  belonging to the 10 pc neighborhood of different HZS. Only two of these 34 bright stars,  $\alpha$ -Carinae (around HD 48265) and  $\alpha$ -Muscae (around TOI-1227), are massive enough ( $\geq 8 M_{\odot}$ ) to pose a noteworthy threat to the habitability (see Section 3.2).

### 3. RESULTS AND DISCUSSIONS

While numerous risks, such as activity-induced stellar winds and superflares from a host star can compromise a planet’s habitability (Airapetian et al. 2017; Garraffo et al. 2017; Rodríguez-Mozos & Moya 2019), here, we examine the possibility of any significant impact from stellar encounters and supernova explosions in the surrounding stellar environment of HZS. These events can significantly alter the habitability of planets by displacing them out of their HZ or by disrupting their atmosphere. Studies have shown that the frequency and proximity of such events has a critical role in the habitability of exoplanets within our galaxy (Lineweaver et al. 2004; Jiménez-Torres et al. 2013; Spitoni et al. 2017; Li et al. 2019, 2020; Spinelli et al. 2021; Rickman et al. 2022; Spinelli & Ghirlanda 2023). These factors further determine the long-term viability of habitable conditions on an exoplanet.

#### 3.1. Stellar Encounters

Stellar encounters can impact exoplanetary systems in various ways (Horner et al. 2020; Davari et al. 2022). A passing star’s gravitational influence can perturb distant objects, such as those in the Oort Cloud, pushing them into highly elliptical orbits that may lead to collisions with inner planets. Closer encounter with neighboring stars can directly destabilize planetary orbits, potentially causing planets to migrate inward, outward, or even escape the system entirely. Such disruptions can also alter the eccentricity and inclination of planetary orbits, reducing the time planets spend in the habitable zone (HZ) and threatening their habitability (Wang et al. 2020; Rickman et al. 2023). In some cases, these perturbations may trigger mechanisms like the Kozai-Lidov effect, leading to oscillations in eccentricity, an-

gular momentum exchange, and changes in orbital inclinations (Naoz 2016; Cai et al. 2017). These orbital shifts may result in variations in stellar insolation flux, which, in turn, can affect a planet’s atmosphere, climate, and potential habitability. Additionally, the destabilization of an outer planet could trigger a cascading effect inward, amplifying instability across planets in the inner orbits. The overall impact of these encounters depends on the mass and proximity of the passing star, as well as the architecture of the planetary system.

Jiménez-Torres et al. (2013) examined the effect of encounters on habitability in various stellar environments of the Milky Way. They simulate different regions by estimating stellar densities and dispersion velocities, creating a model to approximate the number of close flyby events that can potentially alter the orbital dynamics. They showed that a  $1 M_{\odot}$  star passing at a distance of 200 AU can perturb another stellar system with a radius of 100 AU, which has an Oort-like cloud surrounding it. This model is based on the neighborhood’s stellar density, dispersion velocity and evolution time. According to Jiménez-Torres et al. (2013), the number of encounters,  $N_e$  is given by the following equation,

$$N_e = 4\pi n v T_e R^2 \quad (1)$$

where  $N_e$  is the number of encounters,  $R$  is the radius of the stellar system ( $b = 2R$  is the impact parameter<sup>7</sup>),  $n$  is the stellar density in  $\text{pc}^{-3}$ ,  $v$  is the dispersion velocity of the system and  $T_e$  is the evolution time of the system. Although, the evidence for Oort-like clouds around exoplanetary systems is still lacking, it is not uncommon to speculate about their existence (Jiménez-Torres et al. 2013; Baxter et al. 2018; Portegies Zwart et al. 2021). The possibility of planetary bodies residing in Oort-like regions, which can extend up to 100 AU from the host star, has also been suggested (Raymond et al. 2023).

We apply the formalism of Equation (1) to real data (i.e., our HZS sample) and estimate the frequency of gravitational encounters from stars in the 10 pc region of HZS. We used the proper motions and radial velocity of neighborhood stars to calculate the  $U$ ,  $V$  and  $W$  components using PyAstronomy<sup>8</sup> (Czesla et al. 2019; Swastik et al. 2023).  $U$  denotes the velocity toward the galactic center,  $V$  denotes the velocity in the direction of galactic rotation and  $W$  denotes the velocity toward the north galactic pole. Then, we find the dispersion velocity  $v$  from:  $v = \sqrt{\sigma_U^2 + \sigma_V^2 + \sigma_W^2}$ , where  $\sigma$  is the dispersion of the respective components.

<sup>7</sup> The distance of closest approach made by the flyby star to the host star, denoted by  $b$ .

<sup>8</sup> LSR= (8.5, 13.38, 6.49) (Coşkunoğlu et al. 2011)

<sup>6</sup> Hipparcos Catalog 2007

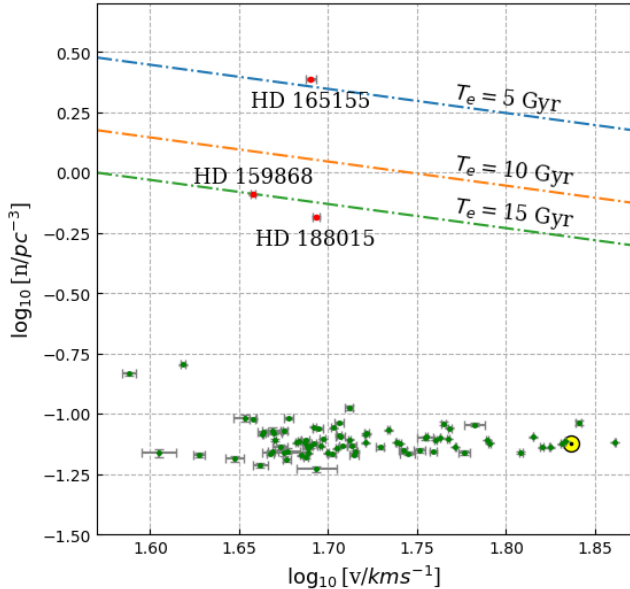


**Figure 5.** A log-log diagram of stellar density versus velocity dispersion. Slanted lines indicate the locus of a single encounter ( $N_e = 1$ ) in stellar density-dispersion parameter space for time scales of 5, 10 and 15 Gyr and  $b = 150$  AU. Three high stellar density environment ( $> 0.4 \text{ pc}^{-3}$ ) are shown by red symbols while the remaining low-encounter HZ systems are indicated by green symbols.

In these calculations, we used the median mass<sup>9</sup> of neighborhood stars to be  $0.3 M_\odot$ , leading to an impact parameter of  $b = 150$  AU. This is inline with peak of the stellar mass function ( $0.3\text{--}0.4 M_\odot$ ), which is consistent with the general prevalence of low-mass M-type stars in the Milky Way and the solar neighborhood (Reylé et al. 2021). The impact parameter  $b = 150$  AU is determined by calculating the distance at which a neighboring star with a mass of  $0.3 M_\odot$  exerts a gravitational force on the exoplanetary Oort cloud that is equal to the force exerted by a  $1 M_\odot$  star at a distance of  $b = 200$  AU. Figure 5 shows a log-scaled plot of stellar density versus dispersion velocity for our sample of 84 HZS. The slanted lines in Figure 5 denote the single encounter thresholds for time scales of 5, 10 and 15 Gyr. This means that for any HZS to experience at least one encounter within a certain time frame, it must lie on or above the slanted line. Since the stellar density around most HZS shown in Figure 5 is low ( $< 0.2 \text{ pc}^{-3}$ ) they are positioned well below the 15 Gyr line and face a negligible threat to habitability from stellar encounters.

<sup>9</sup> Masses have been estimated from the updated (2022) table for spectral sequence based on Pecaut & Mamajaek 2013

Among the 84 systems, three habitable zone stars, namely HD 165155, HD 159868, and HD 188015, are residing in a region with unusually high stellar density ( $> 0.6 \text{ pc}^{-3}$ ) environment compared to Sun and other HZS. This is not surprising, given that these HZS are located near the galactic plane (see Figure 1). However, to rule out erroneous star counts from background contamination and other spurious sources, a further assessment of these three systems is provided in Appendix C.

Notably, HD 165155 is a G8V star with the planet HD 165155 b in the habitable zone (Jenkins et al. 2017). This system has the highest stellar density ( $n \approx 2.45 \text{ pc}^{-3}$ ) in our dataset, with over  $10235 \pm 67$  stars within a 10 pc radius and velocity dispersion  $\approx 49 \text{ kms}^{-1}$ . Given its high-density environment, HD 165155 is expected to undergo at least one stellar encounter within 5 Gyr. In contrast, the other two systems, HD 188015 and HD 159868, have a small likelihood ( $N_e < 1$ ) of experiencing stellar encounters due to their lower stellar density.

Studies on stellar encounters have discussed the evolution of planetary systems in highly dense environments by simulating scenarios with 2000, 8000 and 32000 stars within a virial radius<sup>10</sup> of 1 pc over a span of 50 Myr (Cai et al. 2017). They discuss the survival rates of planets in such environments indicating a clear correlation between survival rates and decreases in stellar density. The work of Bojnordi Arbab & Rahvar (2021) highlighted that the mass and velocity of the flyby stars are crucial in determining the encounter dynamics. Some studies also discuss the formation of HZ planets in clustered environments and their lifetimes with respect to the stellar mass and the stellar densities of their neighborhoods (de Juan Ovelar et al. 2012).

For our HZS sample, the encounter rate was calculated for different  $n$  and  $v$ . Which means the dispersion velocity  $v$  was determined for brighter stars,  $G \lesssim 15$ , for which radial velocity data was available from *Gaia DR3* (see Section 4). Since RV data were not available for the fainter stars, the dispersion velocity obtained is only the lower-limit. However, due to the shallow slope of the single encounter lines in Figure 5, the underestimation of dispersion velocity does not affect the encounter rate in any significant way.

### 3.2. Assessing Threat from SNe Explosions

High-energy particles and radiation arriving from distant regions of space can potentially damage the atmosphere of Earth-like planets or exomoons with an

<sup>10</sup> The radius within which objects exist in a gravitationally bound state.

Earth-like atmosphere. Such radiation originates from high-energy transient phenomena, such as  $\gamma$ -ray bursts and SNe, which involve a brief period of intense radiation that diminishes over time. Our primary focus is to investigate the effects of SNe on the atmospheres of exoplanets or exomoons assuming their atmospheres to be Earth-like (Thomas & Melott 2006; Melott & Thomas 2011; Perkins et al. 2024). The fluence  $F$  received by a planet from a high-energy transient event is given by,

$$F = \frac{\langle E \rangle}{4\pi r^2} \quad (2)$$

where  $\langle E \rangle$  is the characteristic energy of the event and  $r$  is the distance of SNe from the planet (Spinelli et al. 2021; Spinelli & Ghirlanda 2023). The severity of the ozone depletion would depend on the fluence received by the planet. A fluence  $\gtrsim 10 \text{kJm}^{-2}$  would deplete the ozone layer and make the planet vulnerable to harmful radiation and might render the planet uninhabitable (Thomas et al. 2005a,b; Melott & Thomas 2011; Horvath & Galante 2012; Spinelli & Ghirlanda 2023). In our study, we primarily focus on SNe-Ibc and SNe-II since their occurrence is relatively higher than other sources of X and  $\gamma$  radiation such as GRBs and SNe-Ia (Li et al. 2011; Spinelli & Ghirlanda 2023).

It is well established that a Type Ib,c or a Type-II SNe requires a progenitor star with a mass exceeding  $8 M_{\odot}$ . While SNe-Ia are formed from binary accreting systems involving a degenerate star, SNe-Ibc and SNe-II are formed from core-collapse (Spinelli & Ghirlanda 2023). The typical characteristic energy of an SNe ranges from a minimum of  $10^{33}$  kJ (SNe-II) to a maximum of  $10^{37}$  kJ (SNe-I) (Spinelli et al. 2021; Spinelli & Ghirlanda 2023). Therefore, we focus on identifying stars with mass  $\geq 8 M_{\odot}$  within 10 pc of each HZ system, as outlined by Spinelli & Ghirlanda (2023). *Gaia*'s Final Luminosity Age Mass Estimator (FLAME) provides an estimate of stellar mass (Creevey, O. L. et al. 2023; Fouesneau, M. et al. 2023; Gaia Collaboration et al. 2023b), but it is not available for all the stars in our sample. We use the mass-luminosity relationship described by Wang, Jifei & Zhong, Zehao (2018) in Equation (3) to estimate masses for stars in our dataset that lack FLAME-derived mass estimates.

$$\frac{M}{M_{\odot}} = \left( \frac{L}{L_{\odot}} \right)^{\frac{1}{4}} \left( \frac{1}{3} \right)^{(T_{\text{eff}}/T_{\odot})^{\frac{1}{3}} - 1} \quad (3)$$

Here,  $L$  is the luminosity,  $M$  is the mass and  $T_{\text{eff}}$  is the surface temperature of the star. We used Pogson's formula in Equation (3) to calculate luminosity from absolute magnitudes (Pogson 1856; Ibrahim et al.

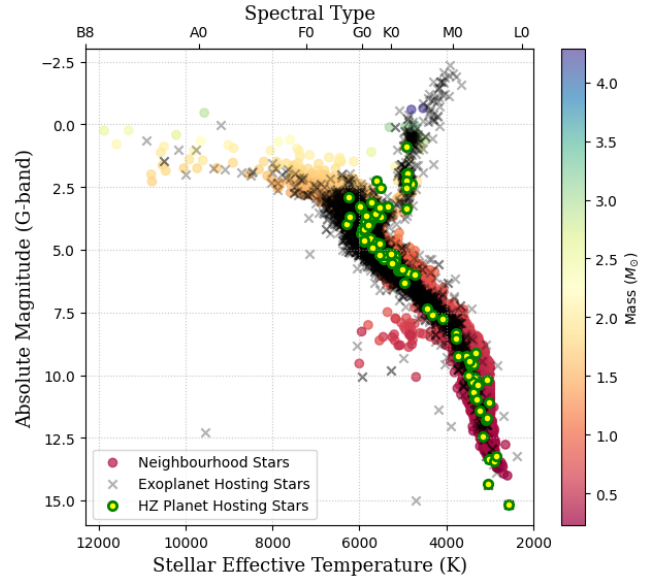


**Figure 6.** HR diagram of all GAIA detected stars in 10 pc region of 84 HZS and the known exoplanet hosting stars. The neighborhood stars are color-coded according to their estimated mass.

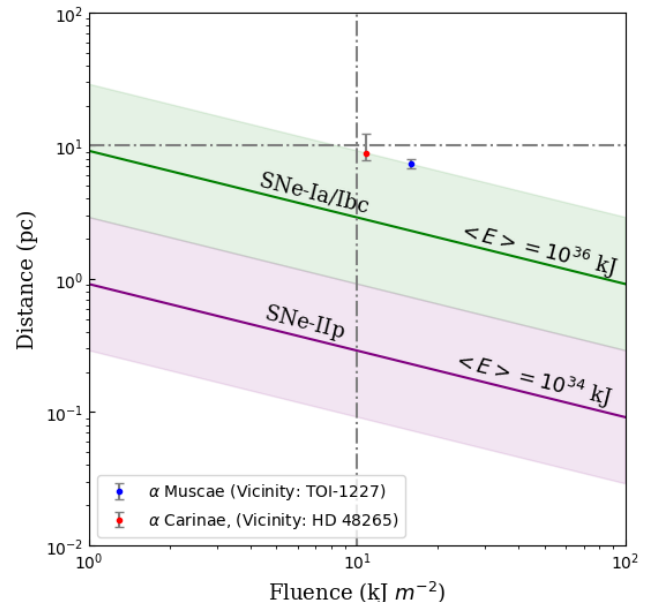


**Figure 7.** Fluence received from SNe explosions as a function of distance. The purple and green bands depict the range of energy released from different SNe. The shaded region to the right of the vertical line receives a fluence in excess of  $10 \text{kJm}^{-2}$ , which is considered harmful to habitability. Locations of two high-mass stars ( $M > 8 M_{\odot}$ ), which are potential progenitors of supernovae, are also shown for comparison.

2018) for stars without FLAME luminosity. In our anal-

ysis of Gaia DR3 dataset we do not find any star with  $M \geq 6 M_{\odot}$  surrounding HZS.

Figure 6 is the Hertzsprung-Russell (HR) diagram of our full Gaia dataset of neighborhood stars. To convert from effective temperature to spectral type, we referred to the updated spectral sequence<sup>11</sup> based on Pecaut & Mamajek (2013). The HR diagram shows that the neighborhood stars in our sample range from L0 to B8-type. Since stars brighter than ( $G \leq 3$ ) are absent in the Gaia catalog, we searched the *Hipparcos* Catalog<sup>12</sup> (Perryman et al. 1997; van Leeuwen 2007) and found 2 HZS (TOI-1227 and HD 48265), having high-mass stars ( $M > 8 M_{\odot}$ ), namely  $\alpha$ -Muscae and  $\alpha$ -Carinae respectively, within their 10 pc vicinity. These stars are potential SNe progenitors. We consider the evolution of these high-mass stars into SNe-Ibc as the worst case scenario from the viewpoint of habitability of the central HZS. The maximum characteristic energy,  $\langle E \rangle$  that a SNe-Ibc would produce is  $\sim 10^{37}$  kJ.

The variation of fluence received from SNe explosions as a function of distance and characteristic energy released is illustrated in Figure 7. In the figure we depict two high-mass stars that are located at a distance  $\lesssim 10$  pc from HZS TOI-1227 and HD 48265. A resulting stellar explosion (SNe-Ibc) releasing a maximum energy  $\langle E \rangle = 10^{37}$  kJ would produce a lethal fluence  $\geq 10$  kJm<sup>-2</sup> of X-rays/ $\gamma$ -rays (Spinelli & Ghirlanda 2023) within 10 pc sphere. The planets in these two systems, namely TOI-1227 b (Mann et al. 2022) and HD 48265 b (Minniti et al. 2009) are gaseous. Although these planets themselves cannot have habitable conditions, they might host exomoons that could have Earth-like atmospheres susceptible to these effects. For an earth-like atmosphere this could deplete  $\sim 68\%$  of the ozone layer (Thomas & Melott 2006; Spinelli et al. 2021).

Note that  $\gamma$ -ray bursts can emit immense energy, affecting planets as far as  $\sim 1$  kpc away (Spinelli et al. 2021; Spinelli & Ghirlanda 2023). However, due to the unpredictability and rarity of  $\gamma$ -ray burst events, we do not consider them within the scope of present work. Similarly, predicting whether a main-sequence white dwarf binary will undergo a Type Ia SNe is challenging, as it depends on factors like their proximity and orbital dynamics of a compact binary system. In contrast, the likelihood of Type Ibc and Type II supernovae is higher in stars with masses  $\geq 8 M_{\odot}$ . In a worst-case scenario, if a high-mass star is stripped of its hydrogen envelope, it will evolve into a SNe-Ib. If both hydro-

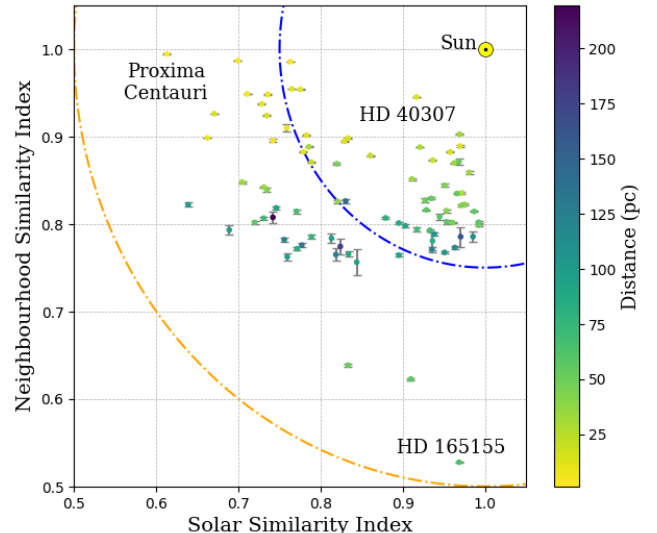


**Figure 8.** Similarity index based comparison of habitable zone systems with solar system. The colorbar represents the distance of HZS from Sun in pc. The blue and orange semicircles centered on the Sun correspond to 0.75 and 0.50 similarity in NSI-SSI plane.

gen and helium are depleted, it will become a SNe-Ic. However, it is rare for a high-mass star to evolve into these categories by losing sufficient hydrogen from its outer layers. In most cases, a high-mass star undergoes core collapse, producing less energetic Type-II supernovae (SNe-II), which indicates their impact is less damaging beyond 5 pc (Melott et al. 2017). None of our HZS have high-mass stars within a 5 pc region. Recent studies also suggest that a SNe explosion occurring even at distances up to 20 pc could be lethal to a planet’s habitability (Thomas & Yelland 2023).

### 3.3. Similarity Indices

The discovery of numerous extrasolar planets has revealed a diverse array of stellar and planetary characteristics, making systematic comparisons crucial for evaluating habitability and assessing the potential for life beyond our solar system. For example, Sun-like stars are more likely to host stable habitable environments for their planetary systems due to the moderate nature of their stellar activity (Loeb et al. 2016; Lingam & Loeb 2017a,b; Haqq-Misra et al. 2018). Additionally, the overall stellar environment of the solar system (e.g., location in the galaxy, neighborhood stellar spectral types, density and dispersion velocity) appears conducive to the long-term maintenance of habitable conditions (Jiménez-Torres et al. 2013; Spitoni et al. 2017; Spinelli et al. 2021; Spinelli & Ghirlanda 2023) and may serve as a valuable reference for comparison (Reylé et al. 2021; Reylé et al. 2022). Furthermore, since the Sun has

<sup>11</sup> Updated (2022) table for spectral sequence based on Pecaut & Mamajek 2013

<sup>12</sup> Hipparcos Catalog 2007



| Column Name                 | Unit                    | Description   | Example Value    |
|-----------------------------|-------------------------|---|------------------|
| Host_Star                   | -                       | Name of host star   | HD 165155        |
| designation                 | -                       | Gaia DR3 identifier   | Gaia DR3 4050... |
| ra                          | degrees                 | Right ascension   | 271.49           |
| dec                         | degrees                 | Declination   | -29.92           |
| parallax                    | mas                     | Parallax  | 15.78            |
| pm_ra                       | mas/yr                  | RA proper motion  | 76.89            |
| pm_dec                      | mas/yr                  | Dec proper motion   | -1.57            |
| radial_velocity             | kms <sup>-1</sup>       | Radial velocity   | 15.3             |
| phot_g_mean_mag             | G-mag                   | Photometric G-band magnitude                                    | 9.22             |
| s_teff                      | K                       | Surface temperature of host star from NEA                       | 5426             |
| s_logg                      | log(cms <sup>-2</sup> ) | Surface gravity of host star from NEA                           | 4.49             |
| s_mul                       | -                       | Number of stars in the system                                   | 1                |
| absolute_mag                | G-mag                   | Absolute magnitude in G-band                                    | 5.21             |
| S.S.I                       | -                       | Solar similarity index  | 0.97             |
| Dispersion_Velocity_log     | log(kms <sup>-1</sup> ) | Log of dispersion velocity of neighborhood stars                | 1.690            |
| Dispersion_Velocity_log_std | log(kms <sup>-1</sup> ) | Uncertainty in log of dispersion velocity of neighborhood stars | 0.003            |
| Object_Den_log              | log(pc <sup>-3</sup> )  | Log of object density of neighborhood stars                     | 0.388            |
| Object_Den_log_std          | log(pc <sup>-3</sup> )  | Uncertainty in log of object density of neighborhood stars      | 0.003            |
| Number                      | -                       | Number of neighborhood stars                                    | 10235            |
| Number_std                  | -                       | Uncertainty in number of neighborhood stars                     | 67               |
| D_Teff                      | K                       | Dispersion in T <sub>eff</sub> for neighborhood stars           | 671              |
| M_Teff                      | K                       | Median of T <sub>eff</sub> for neighborhood stars               | 3324             |
| D_logg                      | log(cms <sup>-2</sup> ) | Dispersion in log <i>g</i> for neighborhood stars               | 0.27             |
| M_logg                      | log(cms <sup>-2</sup> ) | Median of log <i>g</i> for neighborhood stars                   | 4.81             |
| D_Ab_Mag                    | G-mag                   | Dispersion in absolute mag of neighborhood stars                | 1.05             |
| M_Ab_Mag                    | G-mag                   | Median of absolute mag of neighborhood stars                    | 15.49            |
| N.S.I                       | -                       | Neighborhood similarity index                                   | 0.527            |
| NSI_std                     | -                       | Uncertainty in neighborhood similarity index                    | 0.001            |

**Table 1.** Description of the content of the table of 84 HZS (with HD 165155 as an example). ‘Neighborhood stars’ refers to the stars present within the 10 pc environment of the respective HZS. The entire table is available in machine-readable format.

played a crucial role in the evolution and maintenance of life on Earth, assessing the similarity of other planet-hosting stars to the Sun is of paramount importance.

The similarity index is a numerical metric used to quantify the likeness or resemblance between objects or systems sharing specific properties. This concept has been previously applied to assess the resemblance of known extrasolar planets to Earth by comparing their mass, radius, and surface temperature (Cha 2007; Schulze-Makuch et al. 2011). In this study, we employ the concept of similarity index to assess the resemblance and dissimilarity between 84 habitable systems and their stellar environments. Specifically, we utilize two distinct similarity indices:

1. **Solar Similarity Index (SSI):** This index allows for a comparison of the properties of our Solar System with those of corresponding HZS.

2. **Neighborhood Similarity Index (NSI):** This index facilitates a comparison of the properties of stars in the 10 pc volume around Solar System and the neighborhood stars of the HZS.

We define each similarity index as:

$$SSI, NSI = 1 - \sqrt{\frac{1}{n} \sum_{i=1}^n \left( \frac{P_i - P_{i\odot}}{P_i + P_{i\odot}} \right)^2} \quad (4)$$

where  $P_i$  refers to the value of the  $i$ -th stellar parameter chosen for comparison while  $P_{i\odot}$  is the corresponding value for the Sun or the solar system and  $n$  denotes the number of parameters considered.

To calculate the SSI using Equation (4) we selected four parameters, namely, stellar multiplicity, effective temperature, surface gravity and absolute magnitude. Likewise, to calculate the NSI for each HZS, we chose eight parameters for the ensemble of stars within the

10 pc region. These parameters include the dispersion velocity of stars ( $\sigma_v$ ), the median and standard deviation of temperature ( $\langle T_{\text{eff}} \rangle$  and  $\sigma_{T_{\text{eff}}}$ ), the median and standard deviation of absolute magnitude ( $\langle \text{mag} \rangle$  and  $\sigma_{\text{mag}}$ ), the median and standard deviation of  $\log g$  ( $\langle \log g \rangle$  and  $\sigma_{\log g}$ ), and finally the neighborhood star count.

The SSI was calculated directly from Equation (4) for each HZ star, using stellar parameters taken from NEA. For the NSI of a stellar environment, we used the bootstrap method to generate 100,000 neighborhood configurations. We then derived the NSI value from the median of this sampling distribution and its associated uncertainties from the standard deviation (see Appendix B).

The plot of NSI versus SSI in Figure 8 shows the comparison of different HZS with solar system and stars in their respective 10 pc neighborhood. The HZS within the blue circle represent a similarity greater than 0.75 while those with more than 0.50 similarity fall within the orange circle. Overall, we note that NSI is  $> 0.75$  for most HZS implying a high degree of similarity between the stellar environment of the Sun and the HZ stars. Also, the HZS nearer to the solar neighborhood tend to have a higher NSI due to the presence of a similar population of stars. The differences however, tend to grow with an increase in distance as evident from the vertical color gradient seen in Figure 8. On the other hand, SSI values have a larger spread primarily due to the different spectral types of stars in the HZ sample.

More specifically, in Figure 8 we note that HD 40307, a K2.5V dwarf star with  $T_{\text{eff}} \approx 5000$  K, located 13 pc from the Sun and hosting a  $7.1 M_{\oplus}$  habitable zone planet HD 40307g (Mayor et al. 2009; Tuomi et al. 2013; Brasser et al. 2014), has the highest overall similarity index among the 84 HZS. This system has an NSI of 0.94 and SSI of 0.92 and 5 planets discovered in its system. The NSI of Proxima Centauri is highest because its 10 pc volume significantly overlaps with the stars in the 10 pc neighborhood of the Sun. However, Proxima Centauri is a red-dwarf star ( $T_{\text{eff}} \approx 3000$  K) which is cooler and smaller than the Sun, and it is also part of a multiple star system. These differences contribute to its low SSI seen in Figure 8. Conversely, HD 165155 is a G-type HZ star with a high SSI but low NSI. This is largely due to its densely populated surrounding, containing nearly 10,000 stars, in stark contrast to 315 stars in the 10 pc solar neighborhood.

Exoplanet demographic studies have shown that the solar system is somewhat uncommon in terms of both its planetary properties such as mass, radius, orbital period, eccentricity and distribution in the system, as well as the stellar properties of the Sun (Martin & Livio 2015; Winn & Fabrycky 2015; Zhu & Dong 2021). Many

studies have tried to find stars that closely resemble the Sun particularly in terms of fundamental stellar parameters, activity, rotation rate and elemental abundances (Ramírez et al. 2009; Datson et al. 2015; Mahdi et al. 2016). Our current treatment of the SSI is somewhat simplistic. It is not intended to capture all the nuances and subtleties required to establish or refute the uniqueness of the Sun or the solar system among the known exoplanetary systems. Settling this question – one way or another – would require more data and improved characterization of host stars, which future ground-based and space missions will hopefully provide.

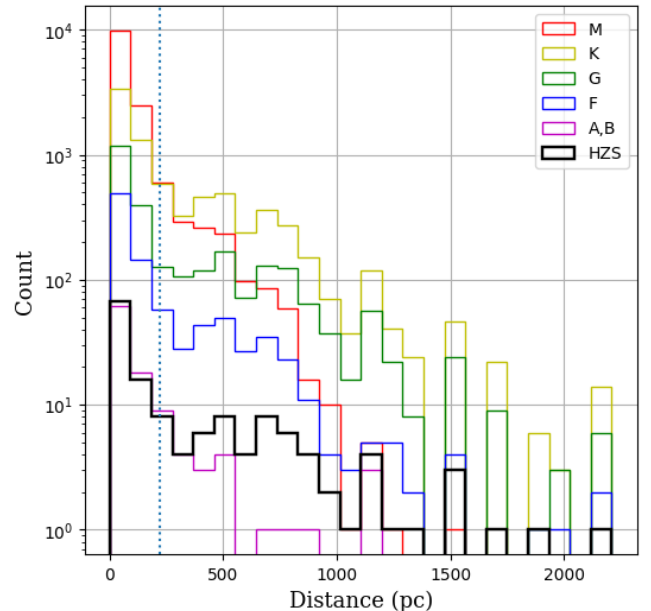


**Figure 9.** Distribution of GAIA-detected neighborhood stars and HZS. The source count is a function of spectral type and distance from the Sun. Eighty four out of 146 HZS studied in this work lie within a distance of 220 pc (marked by a vertical dotted line) from the Sun.

#### 4. COMPLETENESS OF GAIA DATA

Instrument sensitivities limit the detection of stars, as well as the measurement of stellar properties and the quantities derived from them (Fouesneau, M. et al. 2023). Therefore, an instrument is capable of detecting and characterize only a certain fraction of the true number of objects (the ground-truth) – this fraction is called completeness. The completeness of detections and the measurement/estimation of stellar astrophysical parameters (e.g., radial velocity,  $T_{\text{eff}}$ , etc) in *Gaia DR3*, depends on various factors which include source crowding in the field of observation and scanning law (number of visits *Gaia* made to that patch of the sky) (Cantat-Gaudin, Tristan et al. 2023). This affects the accuracy

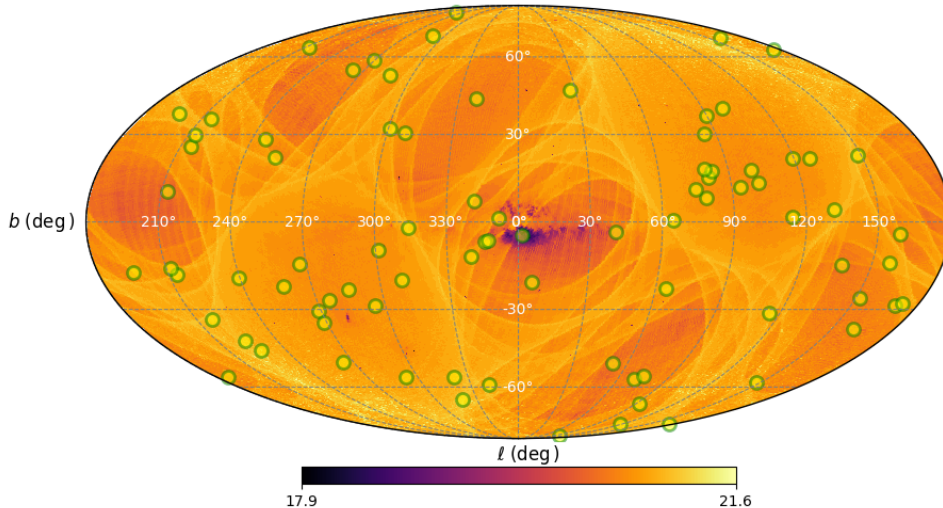


**Figure 10.** The 95% completeness map of the Gaia-scanned region in Galactic coordinates ( $l$  and  $b$ ), generated using the `gaiaunlimited` package (Cantat-Gaudin, Tristan et al. 2023). The color scale indicates the faintest G magnitude at which the 95% completeness threshold is achieved. Our sample of 84 HZS (green circles) has been overlaid on the map to visually depict the completeness of their respective neighborhoods.

of our results outlined in the previous section. In the following subsections, we discuss the completeness of our sample and its impact on threat assessment from stellar encounters and the interpretation of similarity indices.

#### 4.1. Detection Completeness

Stellar encounters heavily depend on the density of the stellar neighborhood; the number of stars is one of the parameters required to calculate the NSI. *Gaia* is sensitive to detect objects with apparent magnitudes ranging from  $G \approx 3$  to  $G \approx 21$  (Evans et al. 2018). Based on the simplified assumption that the solar neighborhood is a good representative of the demographics of stars within  $\sim 250$  pc, we can conclude that bright stars constitute a small fraction of the population whereas low-mass M-dwarfs and ultra-cool dwarfs constitute majority of the population (Reyl e et al. 2021). Figure 9 shows the demographics of the *Gaia* detected 10 pc sample of neighborhood stars as a function of spectral types and distance from the Sun. At closer distances, the detection of most stars is nearly complete. The detection sensitivity begins to decline as the distance increases; however, this decline is faster for late spectral-type stars than for early spectral-type stars. Although T5 dwarfs have been detected in our sample up to 20 pc and the faintest source detected at 240 pc is an M8 dwarf, this doesn’t guarantee a complete detection of similar sources. A single detection may be attributed to *Gaia*’s large number of visits to the corresponding patch of sky or to a relatively darker background (Cantat-Gaudin, Tristan et al. 2023). In reality, there might be many more M-

dwarfs and brown dwarfs in a given region than the few detections suggest.

The completeness of *Gaia DR3* was derived by Cantat-Gaudin, Tristan et al. (2023) by comparing detections of *Gaia DR3* against that of DECaPS<sup>13</sup> (Saydjari et al. 2023). *Gaia* has a complex “scanning law”, and its performance varies significantly between sparse and densely populated regions of the sky. Therefore, the number of useful visits, and hence the total integration time of *Gaia*, is not the same throughout the sky. These factors result in anisotropy of the median magnitude of stars detected by *Gaia* in a particular patch of sky. Cantat-Gaudin, Tristan et al. (2023) use the median magnitude of stars<sup>14</sup> ( $M$ ) to account for the anisotropic selection biases of *Gaia* while empirically modeling its completeness. Figure 10 shows the sky distribution of the faintest magnitude of stars in the Galactic reference system, to which *Gaia* is at least 95% complete. This map was generated using the `gaiaunlimited` package developed by Cantat-Gaudin, Tristan et al. (2023). The overlaid green points show the positions of 84 HZS that we analyze. This figure provides a qualitative description of the sky distribution of the apparent magnitude to which a particular HZS’s neighborhood (fixed  $M$ ) is 95% complete.

<sup>13</sup> Dark Energy Camera Plane Survey (DECaPS) was a ground-based deep survey of the southern galactic plane.

<sup>14</sup> Median magnitude of stars with useful visits (the *Gaia* parameter, `astrometric_matched_transits`)  $\gtrsim 10$ , referred to in Cantat-Gaudin, Tristan et al. (2023) as  $M_{10}$ . We refer to it as  $M$  here for simplicity

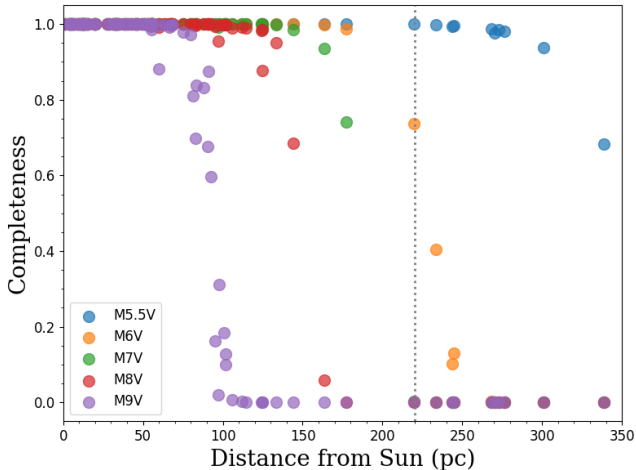


**Figure 11.** *Gaia* completeness of neighborhood stars as a function of distance. Different colors represent different spectral types. Each point corresponds to a HZ system.

DECaPS is a deep survey with a small footprint (6.5% sky coverage). Also, it is not complete to the faintest brown dwarfs and therefore, does not represent the ground truth. Although it can provide a good reference to estimate *Gaia*'s overall completeness, this method is not entirely reliable for computing the true counts for neighborhoods of individual HZS. We therefore, have used a selection function<sup>15</sup>, (see section 2.3 of Cantat-Gaudin, Tristan et al. (2023)) to estimate the completeness as a function of spectral type of stars in HZS neighborhoods.

For a particular spectral type, (i.e., certain absolute  $G$  magnitude) apparent magnitude increases with distance. For every HZ system, (different  $M$ : varying galactic co-ordinates) we compute the completeness using the selection function developed by Cantat-Gaudin, Tristan et al. (2023). Figure 11 shows how the completeness of neighborhood stars of different spectral types varies with distance. Notably, the detection of all stars up to the M-spectral type is nearly complete for HZS within  $\sim 80$  pc from the Sun. The location of the farthest exoplanetary system analyzed in our HZ sample, *Kepler-296*, is marked by a vertical line drawn at 220 pc in Figure 11. We note that the stellar neighborhood of *Kepler-296* is almost complete for M5.5V type stars,  $\sim 70\%$  complete for M6V type, whereas ultra-cool dwarfs (later than M6V types) have a significantly lower likelihood of being detected.

#### 4.2. Completeness of Astrophysical Parameters

The three main instruments onboard *Gaia* include an astrometric instrument for precise stellar position and parallax measurements, a broadband photometer for measuring stellar brightness, and a radial velocity spectrometer to determine the velocity of stars along the line of sight. The radial velocity spectra (RVS) is also used to estimate parameters like  $T_{\text{eff}}$  and  $\log g$ . The photometric instrument provides the color information along with apparent magnitude,  $T_{\text{eff}}$  and  $\log g$ . Recio-Blanco et al. (2023); Creevey, O. L. et al. (2023) and Foesneau, M. et al. (2023) provide a detailed discussion on *Gaia*'s estimates and accuracy of astrophysical parameters. Generally, the stellar parameters obtained using RVS are more accurate than those obtained using photometry. *Gaia* uses three methods to estimate  $T_{\text{eff}}$  and  $\log g$ : Generalized Stellar Parametrizer (GSP), Extended Stellar Parametrizer (ESP), and Multiple Star Classifier (MSC). We obtained the stellar parameters of neighborhood stars from *Gaia* by following the priority order (from highest to lowest): GSP-Spec, GSP-Phot, ESP-HS, ESP-UCD, MSC-1, MSC-2<sup>16</sup>. GSP-Spec mainly operates on stars with  $G \lesssim 15$ , GSP-Phot on  $G \lesssim 19$ , MSC on  $G \lesssim 18.25$ , and ESP-HS and ESP-UCD operate on hot stars and ultra-cool dwarfs, respectively (Recio-Blanco et al. 2023; Creevey, O. L. et al. 2023; Foesneau, M. et al. 2023).

<sup>16</sup> Spec: Spectroscopy, Phot: Photometry, HS: Hot Stars, UCD: Ultra-cool Dwarfs

<sup>15</sup> Empirical model for *Gaia* completeness: a sigmoid function with  $M$  and apparent magnitude as its parameters

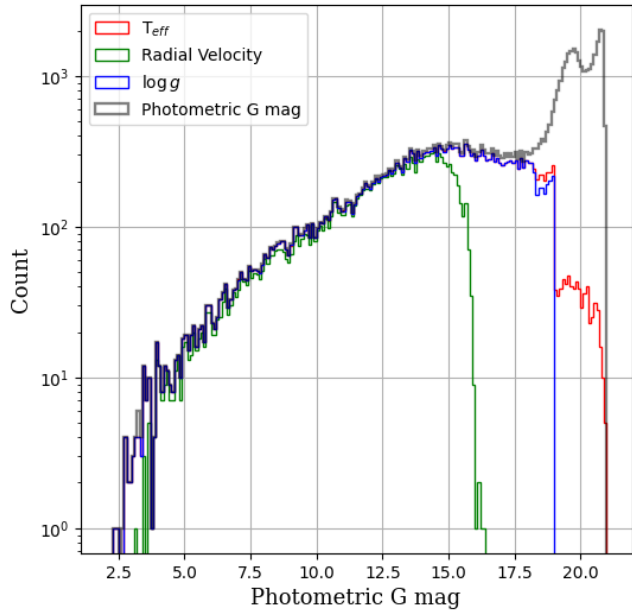


**Figure 12.** Distribution of photometric mean  $G$  magnitude for objects with available  $T_{\text{eff}}$ ,  $\log g$  and radial velocity in *Gaia*.

Figure 12 illustrates the completeness of various astrophysical parameters obtained from *Gaia* as a function of apparent  $G$  magnitude of stars. Notably, the data for most parameters is complete up to  $G \approx 15$ . Beyond that the completeness differs for each parameter. For example, the complete radial velocity data is only available for stars with  $G \lesssim 15$ , whereas  $T_{\text{eff}}$  and  $\log g$  data is available for the majority of stars detected up to  $G \lesssim 17.5$ . These magnitude limits are further described in Fouesneau, M. et al. (2023).

The foregoing discussions demonstrate that our 10 pc neighborhood dataset is incomplete both in terms of source detections and the availability of astrophysical parameters from *Gaia*. This incompleteness directly impacts the results presented in the section 3. For example, a fraction of low-mass faint stars at larger distances would remain undetected, leading to an underestimation of stellar density in the 10 pc region. Consequently, the estimated stellar encounter rates represent a lower limit of the actual values. Likewise, the completeness of astrophysical parameters is biased towards the brighter stars. This indicates that the median values of stellar parameters such as  $T_{\text{eff}}$ ,  $\log g$  derived from their respective bootstrap distributions are overestimated, while the neighborhood star count  $n$ , and absolute magnitude  $M_G$  are underestimated. This introduces a completeness dependent bias in the estimation of NSI. Although this bias in NSI is minimized by restricting our analysis to

the 84 HZS closest to the Sun, it is not entirely eliminated.

## 5. SUMMARY AND CONCLUSION

The quest to find habitable planets is a key area of study in exoplanet research. More than 150 confirmed detections of planets in the habitable zones of various stars have been made. The origin and stability of habitable conditions depend on the star-planet system’s location in the Milky Way and are influenced by factors such as high-energy radiation from supernovae, the presence of heavy elements, and the epoch of planet formation. High rates of catastrophic events in dense stellar regions can hinder the long-term evolution and survival of habitability. For a planet to remain habitable, it must retain its atmosphere, be shielded from harmful radiation, and maintain a stable orbit within its habitable zone without being perturbed by other gravitational influences. The astrophysical impacts of stellar environment is a “low-probability, high-consequence” scenario for the continuation of habitability of exoplanets. Even a single disruptive event of this kind, though less likely, could significantly impact the planet’s habitability.

In this study, we focused on the 10 pc neighborhood around known HZ systems to investigate the potential threats to their habitability from nearby stellar encounters and supernovae. To accomplish these goals, we analyzed the astrometric, photometric, and spectroscopic data of these environments using *Gaia DR3* and *Hipparcos*. We used a bootstrap approach to construct the 10 pc neighborhoods of HZ systems, discussed the influence of stellar environments on habitability and highlighted the limitations due to incomplete *Gaia* data. We also developed two metrics, the Solar Similarity Index and the Neighborhood Similarity Index, to compare the properties of the 10 pc environments of HZ systems with the 10 pc environment of our solar system.

Out of the 84 HZS studied, 3 systems have a stellar density of  $\geq 0.4\text{pc}^{-3}$ . Among these, only one system, HD 165155, has an encounter rate of  $\geq 1$  in 5 Gyr period, increasing the likelihood of perturbation of planetary orbits during the star’s main sequence evolution. We found a high-mass star ( $>8 M_{\odot}$ ) within the 10 pc neighborhoods of each of the two HZS, namely TOI-1227 and HD 48265. These high-mass stars are potential progenitors for supernova explosions. Energy released from these stellar explosions can deposit a high fluence of harmful radiations on distant planets (or their exomoons), stripping off their ozone layer and rendering them uninhabitable. Upon comparing the 10 pc solar and stellar neighborhoods, we find that the stellar environments of the majority of HZS exhibit a high degree of

similarity ( $NSI > 0.75$ ) to the solar neighborhood. Due to the diverse spectral types of HZ planet-hosting stars, when we compare them with the Sun, we get a wide range of SSI values.

Finally, we discussed the possible limitations of this study due to the incompleteness of *Gaia* data. We find that our sample of different HZ system's neighborhood stars is complete to early M-type stars. Incompleteness starts to plague our sample for ultra-cool dwarfs (later than M6V) at  $\sim 220$  pc. We also show that instruments onboard *Gaia* are biased to brighter stars, *Gaia DR3* completely catalogs all astrophysical parameters only till  $G \lesssim 15$ . Therefore, by volume-limiting our sample to 84 HZS within 220 pc, we partially mitigated the uncertainties injected into our analysis due to *Gaia*'s completeness bias. Because of *Gaia* incompleteness, computed stellar encounter probabilities are lower limits and comparison between solar system and the exo-HZS is not accurate. However, our analysis provides a preliminary basis for characterizing the stellar environments of exoplanetary systems and warrants the need for more complete surveys.

From the habitability perspective, investigating the local stellar environments of planet-hosting stars is an interesting and challenging problem that will benefit from more complete and accurate data. The forthcoming *Gaia Data Release 4* (DR4) promises enhanced completeness and precision in estimating the astrophysical parameters of stars, which will improve our capability to

fully characterize the 10 pc neighborhood of HZ stars. Additionally, future deep-sky surveys will further enhance our ability to investigate the stellar neighborhoods of planet-hosting stars at greater distances.

## 6. ACKNOWLEDGEMENT

This work has made use of data from the European Space Agency (ESA) mission *Gaia* (<https://www.cosmos.esa.int/gaia>), processed by the *Gaia* Data Processing and Analysis Consortium (DPAC, <https://www.cosmos.esa.int/web/gaia/dpac/consortium>). Funding for the DPAC has been provided by national institutions, in particular the institutions participating in the *Gaia* Multilateral Agreement. This research has made use of data obtained through the High Energy Astrophysics Science Archive Research Center Online Service, provided by the NASA/Goddard Space Flight Center. This work has also referred the NASA Exoplanet Archive and the Habitable Zone Catalog (Kane & Gelino 2012). This research has made use of the Exoplanet Orbit Database and the Exoplanet Data Explorer at [exoplanets.org](http://exoplanets.org). Tisyagupta would also like to thank the Indian Institute of Astrophysics, for providing the necessary support during this work. Finally, authors sincerely thank the anonymous reviewer for their valuable comments and suggestions, which have helped us improve the quality of this manuscript.

*Software:* NumPy (Harris et al. 2020), PyAstronomy<sup>17</sup> (Czesla et al. 2019), Astroquery (Ginsburg et al. 2019), Matplotlib (Hunter 2007).

## REFERENCES

- Airapetian, V. S., Gloer, A., Khazanov, G. V., et al. 2017, ApJL, 836, L3, doi: [10.3847/2041-8213/836/1/L3](https://doi.org/10.3847/2041-8213/836/1/L3)
- Akeson, R. L., Chen, X., Ciardi, D., et al. 2013, Publications of the Astronomical Society of the Pacific, 125, 989, doi: [10.1086/672273](https://doi.org/10.1086/672273)
- Banerjee, B., Narang, M., Manoj, P., et al. 2024, AJ, 168, 7, doi: [10.3847/1538-3881/ad429f](https://doi.org/10.3847/1538-3881/ad429f)
- Baxter, E. J., Blake, C. H., & Jain, B. 2018, AJ, 156, 243, doi: [10.3847/1538-3881/aae64e](https://doi.org/10.3847/1538-3881/aae64e)
- Bojnordi Arbab, B., & Rahvar, S. 2021, International Journal of Modern Physics D, 30, 2150063, doi: [10.1142/S0218271821500632](https://doi.org/10.1142/S0218271821500632)
- Brasser, R., Ida, S., & Kokubo, E. 2014, Monthly Notices of the Royal Astronomical Society, 440, 3685, doi: [10.1093/mnras/stu555](https://doi.org/10.1093/mnras/stu555)
- Cai, M. X., Kouwenhoven, M. B. N., Portegies Zwart, S. F., & Spurzem, R. 2017, MNRAS, 470, 4337, doi: [10.1093/mnras/stx1464](https://doi.org/10.1093/mnras/stx1464)
- Cantat-Gaudin, Tristan, Fouesneau, Morgan, Rix, Hans-Walter, et al. 2023, A&A, 669, A55, doi: [10.1051/0004-6361/202244784](https://doi.org/10.1051/0004-6361/202244784)
- Cha, S.-H. 2007, City, 1, 1
- Coşkunoglu, B., Ak, S., Bilir, S., et al. 2011, MNRAS, 412, 1237, doi: [10.1111/j.1365-2966.2010.17983.x](https://doi.org/10.1111/j.1365-2966.2010.17983.x)
- Creevey, O. L., Sordo, R., Pailer, F., et al. 2023, A&A, 674, A26, doi: [10.1051/0004-6361/202243688](https://doi.org/10.1051/0004-6361/202243688)
- Czesla, S., Schröter, S., Schneider, C. P., et al. 2019, PyA: Python astronomy-related packages. <http://ascl.net/1906.010>
- Datson, J., Flynn, C., & Portinari, L. 2015, A&A, 574, A124, doi: [10.1051/0004-6361/201425000](https://doi.org/10.1051/0004-6361/201425000)
- Davari, N., Capuzzo-Dolcetta, R., & Spurzem, R. 2022, MNRAS, 513, 90, doi: [10.1093/mnras/stac462](https://doi.org/10.1093/mnras/stac462)

<sup>17</sup> <https://github.com/sczesla/PyAstronomy>

- Davison, A. C., Hinkley, D. V., & Young, G. A. 2003, *Statistical Science*, 18, 141, doi: [10.1214/ss/1063994969](https://doi.org/10.1214/ss/1063994969)
- de Juan Ovelar, M., Kruijssen, J. M. D., Bressert, E., et al. 2012, *A&A*, 546, L1, doi: [10.1051/0004-6361/201219627](https://doi.org/10.1051/0004-6361/201219627)
- Evans, D. W., Riello, M., De Angeli, F., et al. 2018, *A&A*, 616, A4, doi: [10.1051/0004-6361/201832756](https://doi.org/10.1051/0004-6361/201832756)
- Fouesneau, M., Frémat, Y., Andrae, R., et al. 2023, *A&A*, 674, A28, doi: [10.1051/0004-6361/202243919](https://doi.org/10.1051/0004-6361/202243919)
- Fujii, Y., Angerhausen, D., Deitrick, R., et al. 2018, *Astrobiology*, 18, 739, doi: [10.1089/ast.2017.1733](https://doi.org/10.1089/ast.2017.1733)
- Gaia Collaboration, Vallenari, A., Brown, A. G. A., et al. 2023a, *A&A*, 674, A1, doi: [10.1051/0004-6361/202243940](https://doi.org/10.1051/0004-6361/202243940)
- Gaia Collaboration, Creevey, O. L., Sarro, L. M., et al. 2023b, *A&A*, 674, A39, doi: [10.1051/0004-6361/202243800](https://doi.org/10.1051/0004-6361/202243800)
- Garraffo, C., Drake, J. J., Cohen, O., Alvarado-Gómez, J. D., & Moschou, S. P. 2017, *ApJL*, 843, L33, doi: [10.3847/2041-8213/aa79ed](https://doi.org/10.3847/2041-8213/aa79ed)
- Ginsburg, A., Sipőcz, B. M., Brasseur, C. E., et al. 2019, *AJ*, 157, 98, doi: [10.3847/1538-3881/aafc33](https://doi.org/10.3847/1538-3881/aafc33)
- Glaser, D. M., Hartnett, H. E., Desch, S. J., et al. 2020, *The Astrophysical Journal*, 893, 163, doi: [10.3847/1538-4357/ab822d](https://doi.org/10.3847/1538-4357/ab822d)
- Gonzalez, G., Brownlee, D., & Ward, P. 2001, *Icarus*, 152, 185, doi: [10.1006/icar.2001.6617](https://doi.org/10.1006/icar.2001.6617)
- Han, E., Wang, S. X., Wright, J. T., et al. 2014, *PASP*, 126, 827, doi: [10.1086/678447](https://doi.org/10.1086/678447)
- Haqq-Misra, J., Kopparapu, R. K., & Wolf, E. T. 2018, *International Journal of Astrobiology*, 17, 77
- Harris, C. R., Millman, K. J., van der Walt, S. J., et al. 2020, *Nature*, 585, 357, doi: [10.1038/s41586-020-2649-2](https://doi.org/10.1038/s41586-020-2649-2)
- Heller, R. 2012, *A&A*, 545, L8, doi: [10.1051/0004-6361/201220003](https://doi.org/10.1051/0004-6361/201220003)
- Heller, R., & Armstrong, J. 2014, *Astrobiology*, 14, 50, doi: [10.1089/ast.2013.1088](https://doi.org/10.1089/ast.2013.1088)
- Heller, R., & Barnes, R. 2013, *Astrobiology*, 13, 18, doi: [10.1089/ast.2012.0859](https://doi.org/10.1089/ast.2012.0859)
- Hill, M. L., Bott, K., Dalba, P. A., et al. 2023, *The Astronomical Journal*, 165, 34, doi: [10.3847/1538-3881/aca1c0](https://doi.org/10.3847/1538-3881/aca1c0)
- Hill, M. L., Kane, S. R., Seperuelo Duarte, E., et al. 2018, *ApJ*, 860, 67, doi: [10.3847/1538-4357/aac384](https://doi.org/10.3847/1538-4357/aac384)
- Horner, J., Kane, S. R., Marshall, J. P., et al. 2020, *PASP*, 132, 102001, doi: [10.1088/1538-3873/ab8eb9](https://doi.org/10.1088/1538-3873/ab8eb9)
- Horvath, J. E., & Galante, D. 2012, *International Journal of Astrobiology*, 11, 279–286, doi: [10.1017/S1473550412000304](https://doi.org/10.1017/S1473550412000304)
- Hunter, J. D. 2007, *Computing in Science & Engineering*, 9, 90, doi: [10.1109/MCSE.2007.55](https://doi.org/10.1109/MCSE.2007.55)
- Ibrahim, I., Malasan, H. L., Kunjaya, C., et al. 2018, *Research in Astronomy and Astrophysics*, 18, 041, doi: [10.1088/1674-4527/18/4/41](https://doi.org/10.1088/1674-4527/18/4/41)
- Jenkins, J. S., Jones, H. R. A., Tuomi, M., et al. 2017, *MNRAS*, 466, 443, doi: [10.1093/mnras/stw2811](https://doi.org/10.1093/mnras/stw2811)
- Jiménez-Torres, J. J., Pichardo, B., Lake, G., & Segura, A. 2013, *Astrobiology*, 13, 491, doi: [10.1089/ast.2012.0842](https://doi.org/10.1089/ast.2012.0842)
- Kane, S. R., & Gelino, D. M. 2012, *PASP*, 124, 323, doi: [10.1086/665271](https://doi.org/10.1086/665271)
- Kasting, J. F., Whitmire, D. P., & Reynolds, R. T. 1993, *Icarus*, 101, 108, doi: [https://doi.org/10.1006/icar.1993.1010](https://doi.org/https://doi.org/10.1006/icar.1993.1010)
- Kopparapu, R. K., Ramirez, R. M., SchottelKotte, J., et al. 2014, *The Astrophysical Journal*, 787, L29, doi: [10.1088/2041-8205/787/2/L29](https://doi.org/10.1088/2041-8205/787/2/L29)
- Kopparapu, R. K., Ramirez, R., Kasting, J. F., et al. 2013, *The Astrophysical Journal*, 765, 131, doi: [10.1088/0004-637X/765/2/131](https://doi.org/10.1088/0004-637X/765/2/131)
- Li, D., Mustill, A. J., & Davies, M. B. 2019, *Monthly Notices of the Royal Astronomical Society*, 488, 1366, doi: [10.1093/mnras/stz1794](https://doi.org/10.1093/mnras/stz1794)
- . 2020, *Monthly Notices of the Royal Astronomical Society*, 496, 1149, doi: [10.1093/mnras/staa1622](https://doi.org/10.1093/mnras/staa1622)
- Li, W., Leaman, J., Chornock, R., et al. 2011, *MNRAS*, 412, 1441, doi: [10.1111/j.1365-2966.2011.18160.x](https://doi.org/10.1111/j.1365-2966.2011.18160.x)
- Lineweaver, C. H., Fenner, Y., & Gibson, B. K. 2004, *Science*, 303, 59
- Lingam, M., & Loeb, A. 2017a, *The Astrophysical Journal*, 848, 41, doi: [10.3847/1538-4357/aa8e96](https://doi.org/10.3847/1538-4357/aa8e96)
- . 2017b, *The Astrophysical Journal Letters*, 846, L21, doi: [10.3847/2041-8213/aa8860](https://doi.org/10.3847/2041-8213/aa8860)
- Lisse, C. M., Desch, S. J., Unterborn, C. T., et al. 2020, *The Astrophysical Journal Letters*, 898, L17, doi: [10.3847/2041-8213/ab9b91](https://doi.org/10.3847/2041-8213/ab9b91)
- Loeb, A., Batista, R. A., & Sloan, D. 2016, *Journal of Cosmology and Astroparticle Physics*, 2016, 040
- Mahdi, D., Soubiran, C., Blanco-Cuaresma, S., & Chemin, L. 2016, *A&A*, 587, A131, doi: [10.1051/0004-6361/201527472](https://doi.org/10.1051/0004-6361/201527472)
- Mann, A. W., Wood, M. L., Schmidt, S. P., et al. 2022, *AJ*, 163, 156, doi: [10.3847/1538-3881/ac511d](https://doi.org/10.3847/1538-3881/ac511d)
- Martin, R. G., & Livio, M. 2015, *The Astrophysical Journal*, 810, 105, doi: [10.1088/0004-637X/810/2/105](https://doi.org/10.1088/0004-637X/810/2/105)
- Mayor, M., Udry, S., Lovis, C., et al. 2009, *A&A*, 493, 639, doi: [10.1051/0004-6361:200810451](https://doi.org/10.1051/0004-6361:200810451)
- Melott, A. L., & Thomas, B. C. 2011, *Astrobiology*, 11, 343, doi: [10.1089/ast.2010.0603](https://doi.org/10.1089/ast.2010.0603)
- Melott, A. L., Thomas, B. C., Kachelrieß, M., Semikoz, D. V., & Overholt, A. C. 2017, *ApJ*, 840, 105, doi: [10.3847/1538-4357/aa6c57](https://doi.org/10.3847/1538-4357/aa6c57)

- Minniti, D., Butler, R. P., López-Morales, M., et al. 2009, *ApJ*, 693, 1424, doi: [10.1088/0004-637X/693/2/1424](https://doi.org/10.1088/0004-637X/693/2/1424)
- Naoz, S. 2016, *ARA&A*, 54, 441, doi: [10.1146/annurev-astro-081915-023315](https://doi.org/10.1146/annurev-astro-081915-023315)
- Narang, M., Manoj, P., Furlan, E., et al. 2018, *AJ*, 156, 221, doi: [10.3847/1538-3881/aae391](https://doi.org/10.3847/1538-3881/aae391)
- Narang, M., Oza, A. V., Hakim, K., et al. 2023, *AJ*, 165, 1, doi: [10.3847/1538-3881/ac9eb8](https://doi.org/10.3847/1538-3881/ac9eb8)
- NASA Exoplanet Science Institute. 2020, Planetary Systems Table, IPAC, doi: [10.26133/NEA12](https://doi.org/10.26133/NEA12)
- Pecaut, M. J., & Mamajek, E. E. 2013, *ApJS*, 208, 9, doi: [10.1088/0067-0049/208/1/9](https://doi.org/10.1088/0067-0049/208/1/9)
- Perkins, H. M. L., Ellis, J., Fields, B. D., et al. 2024, *The Astrophysical Journal*, 961, 170, doi: [10.3847/1538-4357/ad12b7](https://doi.org/10.3847/1538-4357/ad12b7)
- Perryman, M. A. C., Lindegren, L., Kovalevsky, J., et al. 1997, *A&A*, 323, L49
- Pogson, N. 1856, *MNRAS*, 17, 12, doi: [10.1093/mnras/17.1.12](https://doi.org/10.1093/mnras/17.1.12)
- Portegies Zwart, S., Torres, S., Cai, M. X., & Brown, A. G. A. 2021, *A&A*, 652, A144, doi: [10.1051/0004-6361/202040096](https://doi.org/10.1051/0004-6361/202040096)
- Ramachandran, K. M., & Tsokos, C. P. 2021, in *Mathematical Statistics with Applications in R (Third Edition)*, third edition edn., ed. K. M. Ramachandran & C. P. Tsokos (Academic Press), 531–568, doi: <https://doi.org/10.1016/B978-0-12-817815-7.00013-0>
- Ramírez, I., Meléndez, J., & Asplund, M. 2009, *A&A*, 508, L17, doi: [10.1051/0004-6361/200913038](https://doi.org/10.1051/0004-6361/200913038)
- Raymond, S. N., Izidoro, A., & Kaib, N. A. 2023, *MNRAS*, 524, L72, doi: [10.1093/mnras/524/1/L72](https://doi.org/10.1093/mnras/524/1/L72)
- Recio-Blanco, A., de Laverny, P., Palicio, P. A., et al. 2023, *A&A*, 674, A29, doi: [10.1051/0004-6361/202243750](https://doi.org/10.1051/0004-6361/202243750)
- Redfield, S., Batalha, N., Benneke, B., et al. 2024, *arXiv e-prints*, arXiv:2404.02932, doi: [10.48550/arXiv.2404.02932](https://doi.org/10.48550/arXiv.2404.02932)
- Reylé, C., Jardine, K., Fouqué, P., et al. 2021, *Astronomy & Astrophysics*, 650, A201, doi: [10.1051/0004-6361/202140985](https://doi.org/10.1051/0004-6361/202140985)
- Reylé, C., Jardine, K., Fouqué, P., et al. 2021, *A&A*, 650, A201, doi: [10.1051/0004-6361/202140985](https://doi.org/10.1051/0004-6361/202140985)
- Reylé, C., Jardine, K., Fouqué, P., et al. 2022, in *The 21st Cambridge Workshop on Cool Stars, Stellar Systems, and the Sun*, Cambridge Workshop on Cool Stars, Stellar Systems, and the Sun, 218, doi: [10.5281/zenodo.7669746](https://doi.org/10.5281/zenodo.7669746)
- Rickman, H., Wajer, P., Przyłuski, R., et al. 2023, *MNRAS*, 520, 637, doi: [10.1093/mnras/stac3705](https://doi.org/10.1093/mnras/stac3705)
- Rickman, H., Wajer, P., Przyłuski, R., et al. 2022, *Monthly Notices of the Royal Astronomical Society*, 520, 637, doi: [10.1093/mnras/stac3705](https://doi.org/10.1093/mnras/stac3705)
- Rodríguez-Mozos, J. M., & Moya, A. 2019, *A&A*, 630, A52, doi: [10.1051/0004-6361/201935543](https://doi.org/10.1051/0004-6361/201935543)
- Rybizki, J., Green, G. M., Rix, H.-W., et al. 2022, *MNRAS*, 510, 2597, doi: [10.1093/mnras/stab3588](https://doi.org/10.1093/mnras/stab3588)
- Saydjari, A. K., Schlafly, E. F., Lang, D., et al. 2023, *ApJS*, 264, 28, doi: [10.3847/1538-4365/aca594](https://doi.org/10.3847/1538-4365/aca594)
- Schneider, J., Dedieu, C., Le Sidaner, P., Savalle, R., & Zolotukhin, I. 2011, *A&A*, 532, A79, doi: [10.1051/0004-6361/201116713](https://doi.org/10.1051/0004-6361/201116713)
- Schulze-Makuch, D., Méndez, A., Fairén, A. G., et al. 2011, *Astrobiology*, 11, 1041, doi: [10.1089/ast.2010.0592](https://doi.org/10.1089/ast.2010.0592)
- Schwieterman, E. W., Kiang, N. Y., Parenteau, M. N., et al. 2018, *Astrobiology*, 18, 663, doi: [10.1089/ast.2017.1729](https://doi.org/10.1089/ast.2017.1729)
- Spinelli, R., & Ghirlanda, G. 2023, *Universe*, 9, doi: [10.3390/universe9020060](https://doi.org/10.3390/universe9020060)
- Spinelli, R., Ghirlanda, G., Haardt, F., Ghisellini, G., & Scuderi, G. 2021, *Astronomy & Astrophysics*, 647, A41
- Spitoni, E., Gioannini, L., & Matteucci, F. 2017, *Astronomy & Astrophysics*, 605, A38
- Stark, C. C., Roberge, A., Mandell, A., & Robinson, T. D. 2014, *The Astrophysical Journal*, 795, 122, doi: [10.1088/0004-637X/795/2/122](https://doi.org/10.1088/0004-637X/795/2/122)
- Swastik, C., Banyal, R. K., Narang, M., et al. 2022, *AJ*, 164, 60, doi: [10.3847/1538-3881/ac756a](https://doi.org/10.3847/1538-3881/ac756a)
- . 2021, *AJ*, 161, 114, doi: [10.3847/1538-3881/abd802](https://doi.org/10.3847/1538-3881/abd802)
- Swastik, C., Banyal, R. K., Narang, M., et al. 2023, *The Astronomical Journal*, 166, 91
- Swastik, C., Banyal, R. K., Narang, M., Unni, A., & Sivarani, T. 2024, *AJ*, 167, 270, doi: [10.3847/1538-3881/ad40ae](https://doi.org/10.3847/1538-3881/ad40ae)
- Thomas, B. C., Jackman, C. H., Melott, A. L., et al. 2005a, *The Astrophysical Journal*, 622, L153, doi: [10.1086/429799](https://doi.org/10.1086/429799)
- Thomas, B. C., & Melott, A. L. 2006, *New Journal of Physics*, 8, 120, doi: [10.1088/1367-2630/8/7/120](https://doi.org/10.1088/1367-2630/8/7/120)
- Thomas, B. C., & Yelland, A. M. 2023, *ApJ*, 950, 41, doi: [10.3847/1538-4357/accf8a](https://doi.org/10.3847/1538-4357/accf8a)
- Thomas, B. C., Melott, A. L., Jackman, C. H., et al. 2005b, *The Astrophysical Journal*, 634, 509, doi: [10.1086/496914](https://doi.org/10.1086/496914)
- Tinetti, G., Drossart, P., Eccleston, P., et al. 2018, *Experimental Astronomy*, 46, 135, doi: [10.1007/s10686-018-9598-x](https://doi.org/10.1007/s10686-018-9598-x)
- Torra, F., Castañeda, J., Fabricius, C., et al. 2021, *A&A*, 649, A10, doi: [10.1051/0004-6361/202039637](https://doi.org/10.1051/0004-6361/202039637)
- Tuomi, M., Anglada-Escudé, G., Gerlach, E., et al. 2013, *A&A*, 549, A48, doi: [10.1051/0004-6361/201220268](https://doi.org/10.1051/0004-6361/201220268)
- Underwood, D. R., Jones, B. W., & Sleep, P. N. 2003, *International Journal of Astrobiology*, 2, 289, doi: [10.1017/S1473550404001715](https://doi.org/10.1017/S1473550404001715)



- Unni, A., Narang, M., Sivarani, T., et al. 2022, *AJ*, 164, 181, doi: [10.3847/1538-3881/ac8b7c](https://doi.org/10.3847/1538-3881/ac8b7c)
- van Leeuwen, F. 2007, *A&A*, 474, 653, doi: [10.1051/0004-6361:20078357](https://doi.org/10.1051/0004-6361:20078357)
- Wang, Y.-H., Perna, R., & Leigh, N. W. C. 2020, *MNRAS*, 496, 1453, doi: [10.1093/mnras/staa1627](https://doi.org/10.1093/mnras/staa1627)
- Wang, Jifei, & Zhong, Zehao. 2018, *A&A*, 619, L1, doi: [10.1051/0004-6361/201834109](https://doi.org/10.1051/0004-6361/201834109)
- Ware, A., Young, P., Truitt, A., & Spacek, A. 2022, *The Astrophysical Journal*, 929, 143, doi: [10.3847/1538-4357/ac5c4e](https://doi.org/10.3847/1538-4357/ac5c4e)
- Winn, J. N., & Fabrycky, D. C. 2015, *ARA&A*, 53, 409, doi: [10.1146/annurev-astro-082214-122246](https://doi.org/10.1146/annurev-astro-082214-122246)
- Zhu, W., & Dong, S. 2021, *ARA&A*, 59, 291, doi: [10.1146/annurev-astro-112420-020055](https://doi.org/10.1146/annurev-astro-112420-020055)

## APPENDIX

## A. FUNCTION TO OBTAIN 25 PC SAMPLES

```

from astroquery.gaia import Gaia as ga

def nearby25(par,dec,ra):
    query = "SELECT * \
            FROM gaiadr3.gaia_source as g\
            JOIN gaiadr3.astrophysical_parameters AS ap ON g.source_id = ap.source_id\
            WHERE SQRT(POWER((1000/g.parallax)*COS(RADIANS(g.dec))*COS(RADIANS(g.ra))\
            - 1000/"+str(par)+"*COS(RADIANS("+str(dec)+"))*COS(RADIANS("+str(ra)+")),2) +\
            POWER((1000/g.parallax)*COS(RADIANS(g.dec))*SIN(RADIANS(g.ra))\
            - 1000/"+str(par)+"*COS(RADIANS("+str(dec)+"))*SIN(RADIANS("+str(ra)+")),2) +\
            POWER((1000/g.parallax)*SIN(RADIANS(g.dec))\
            - 1000/"+str(par)+"*SIN(RADIANS("+str(dec)+")),2)) <= 25 AND g.parallax > 0"

    r = ga.launch_job_async(query)
    res = r.get_results()

    return res

```

The above code defines a function `nearby25` that queries the *Gaia DR3* archive to find stars within a 25 pc radius of a habitable zone system based on its `parallax` (mas), `ra` and `dec`. The *Gaia* parallax ( $\varpi$ ) is converted to the radial distance from the Sun by simple inversion  $r = 1/\varpi$ . The query also joins data from two *GAIA DR3* tables: `gaia_source` and `astrophysical_parameters`, based on a common `source_id`.

The code converts the spherical polar coordinates  $(r, \theta, \phi)$  to Cartesian coordinates  $(x, y, z)$ . It makes the following assumptions to do so:

- The  $x$ -axis extends from the origin  $O$  through the vernal equinox along the equatorial plane. This axis aligns with  $0^\circ$  RA.
- The  $y$ -axis, orthogonal to the  $x$ -axis within the equatorial plane, points towards  $90^\circ$  RA.
- The  $z$ -axis, is perpendicular to the equatorial plane.

To be consistency with spherical geometry, we define,  $\phi = \text{RA}$  (angle made with  $x$ -axis) and  $\theta = 90 - \text{Dec}$  (angle made with  $z$ -axis). These spherical polar coordinates  $(r, \theta, \phi)$  are then converted to Cartesian coordinates  $(x, y, z)$  via the following transformation:

$$\begin{aligned}
 x &= r \sin \theta \cos \phi \\
 y &= r \sin \theta \sin \phi \\
 z &= r \cos \theta
 \end{aligned} \tag{A1}$$

The distance between the HZ star  $(x, y, z)$  and a neighboring star  $(x', y', z')$  in 10 pc region is calculated using:  $d = \sqrt{(x - x')^2 + (y - y')^2 + (z - z')^2}$ . In summary, for each HZ system, the three input parameters – parallax, declination and right ascension define its spatial location. *Gaia DR3* is queried for the spatial locations of stars detected within 25 pc of the HZS using the `nearby25` function which is defined above. This 25 pc volume of stars around a HZ system is then used to construct the 10 pc neighborhood of stars using the bootstrapping algorithm as explained in the Appendix B.

## B. CONSTRUCTING THE 10 PC STELLAR NEIGHBORHOOD USING BOOTSTRAP METHOD

Bootstrapping is a resampling technique employed in statistics to estimate the sampling distribution of a quantity by creating multiple simulated datasets from an original sample. This process involves randomly selecting data points

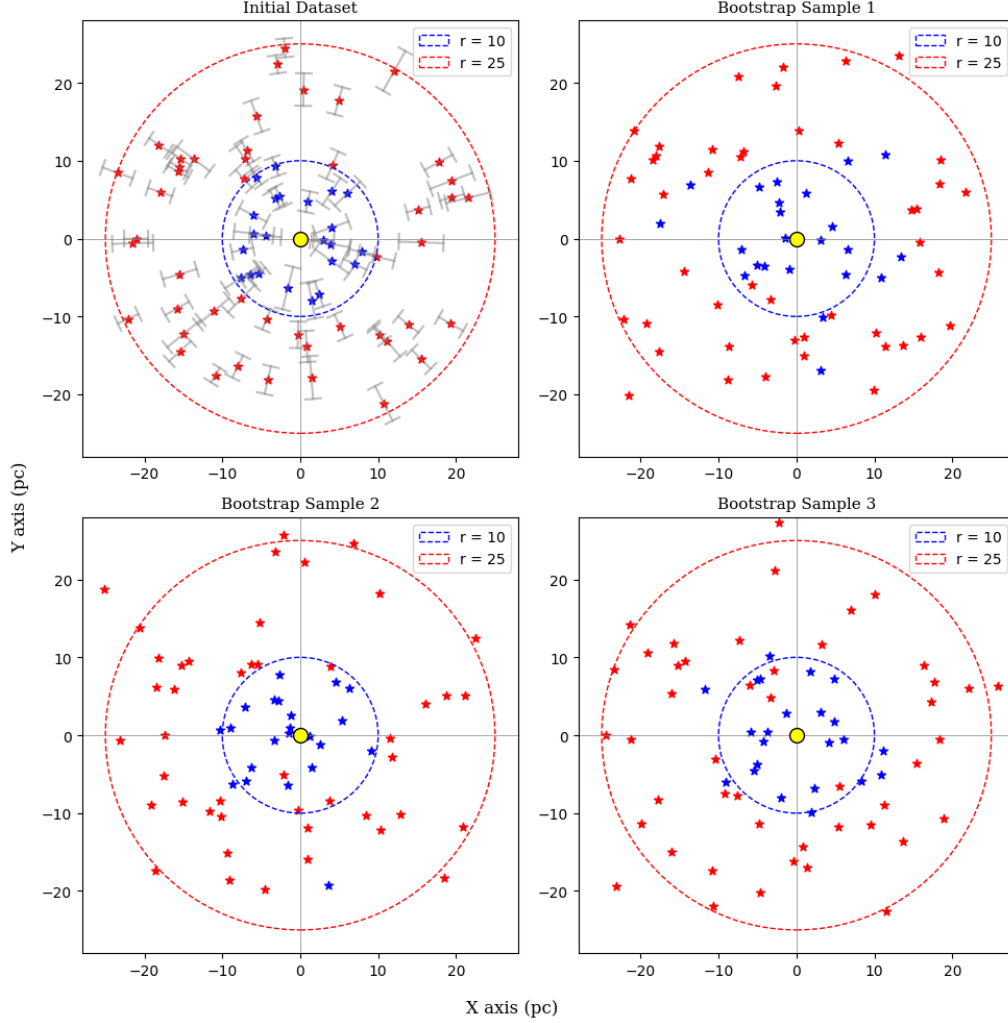


**Figure 13.** Top left: The initial dataset of stars with measured parallaxes ( $\varpi$ ) and  $\pm 1\sigma_{\varpi}$  errors projected on a 2D plane. The blue symbols are stars residing within a 10 pc radius denoted by blue circle and red symbols are stars in 25 pc radius denoted by red circle. Top right panel and bottom row: Three randomly drawn samples from the original distribution showing some of the stars crossing the 10 pc boundary.

from the original dataset with replacement, constructing new samples of the same size as the original (Davison et al. 2003; Ramachandran & Tsokos 2021). To construct the 10 pc neighborhood of each HZS, we applied the bootstrap method to *Gaia*-detected stars within their 25 pc volume. This algorithm is shown as a flowchart in Figure 14. For visualizing how the algorithm resamples to construct new configurations of neighborhoods in each iteration, we consider a hypothetical dataset of  $n$  neighborhood stars (original 25 pc data from *Gaia*) with known parallaxes and parallax errors as shown in the upper left panel of Figure 13. The blue and red circles represent the 10 pc and the 25 pc neighborhood boundary, respectively. We assume the measured parallax of each star  $j$  follows the Gaussian distribution  $\mathcal{N}_j(\varpi_j, \sigma_{\varpi j})$ , where  $\varpi_j$  is the mean parallax and  $\sigma_{\varpi j}$  is the standard deviation. In bootstrap, we randomly draw  $n$  stars from the original sample  $\{\mathcal{N}_j(\varpi_j, \sigma_{\varpi j})\}_{j=1}^n$  and select those for which  $r = 1/\varpi \leq 10$  pc. Applying this cutoff cause some stars originally outside the 10 pc boundary to move inside, while some stars initially within the boundary to move beyond the 10 pc limit. This creates a new sample of 10 pc neighborhood. Three random realizations of bootstrap process are illustrated in top-right panel and the bottom row of Figure 13. The likelihood of a star crossing the 10 pc boundary strongly depends on the original parallax  $\varpi$  and the associated parallax error  $\sigma_{\varpi}$ . This means that, for each random draw, stars near the 10 pc boundary in the original sample are more likely to move in and out of the 10 pc region compared to stars significantly closer to or farther from the center. For each iteration we count the number of stars in 10 pc region and also keep track of their astrophysical parameters. After  $10^5$  bootstrap runs we

get a sampling distribution of each parameter. The median and standard deviation of these distributions are taken as parameters of interest (e.g., dispersion velocity, number density, etc).

This is a quantitative way to statistically estimate the uncertainties introduced by parallax errors in constructing the 10 pc neighborhood of HZS. The bootstrapping algorithm described above provides us with the sampling distribution of neighborhood astrophysical parameters used for our analysis. For example, the results for a system HD 165155 have been shown in Figure 15. For more than 20000 realizations, the neighborhood is found to have 10200 stars, while on none of the occasions do we find 10500 or more stars. The median and standard deviation have been obtained from these sampling distributions for star count and astrophysical parameters such as  $\langle \log g \rangle$ ,  $\langle T_{\text{eff}} \rangle$ , and  $\langle \text{Absolute Magnitude} \rangle$ . We conclude from this analysis that HD 165155 has  $10235 \pm 67$  stars with a median  $T_{\text{eff}}$  of  $3324 \pm 28$  K, median  $\log g$  of  $4.81 \pm 0.01$  and median absolute magnitude of  $15.490 \pm 0.003$ . The astrophysical parameters of all 84 HZS and their 10 pc neighborhood stars, estimated using bootstrap, are provided in the machine-readable table.

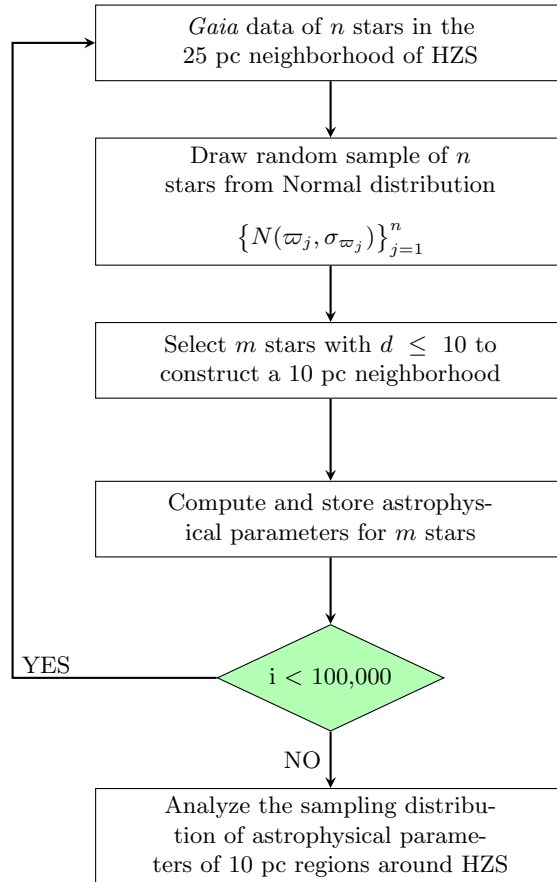


**Figure 14.** Schematic of the bootstrapping algorithm used for constructing a 10 pc neighborhood of HZ planet-hosting stars.

### C. 10 PC NEIGHBORHOODS WITH HIGH DENSITIES

We have studied the 10 pc neighborhood of 84 HZS and identified three systems—HD 165155, HD 159868, and HD 188015—that stand out due to their unusually high star densities. HD 165155, located  $\sim 63$  pc away, with  $\sim 10,000$  stars in its 10 pc vicinity, has a local neighborhood star density 30 times larger than the Sun and the majority of other HZS studied. HD 159868 and HD 188015, while showing lower densities, still contain  $\sim 3,400$  and  $\sim 2,700$  stars, respectively, which is about 10 times greater than the local density of the Sun’s neighborhood. Given their positions at or near the galactic plane, these high-density regions might initially seem unrealistic, raising the possibility of inclusion of spurious sources or contamination of the sample by the background stars. Such artifacts can also arise from diffraction spikes of bright stars, source confusion, faults in telescope behavior, or transiting solar system objects (Torra et al. 2021). We carefully analyzed these high-density regions to address the serious concern of sample contamination.

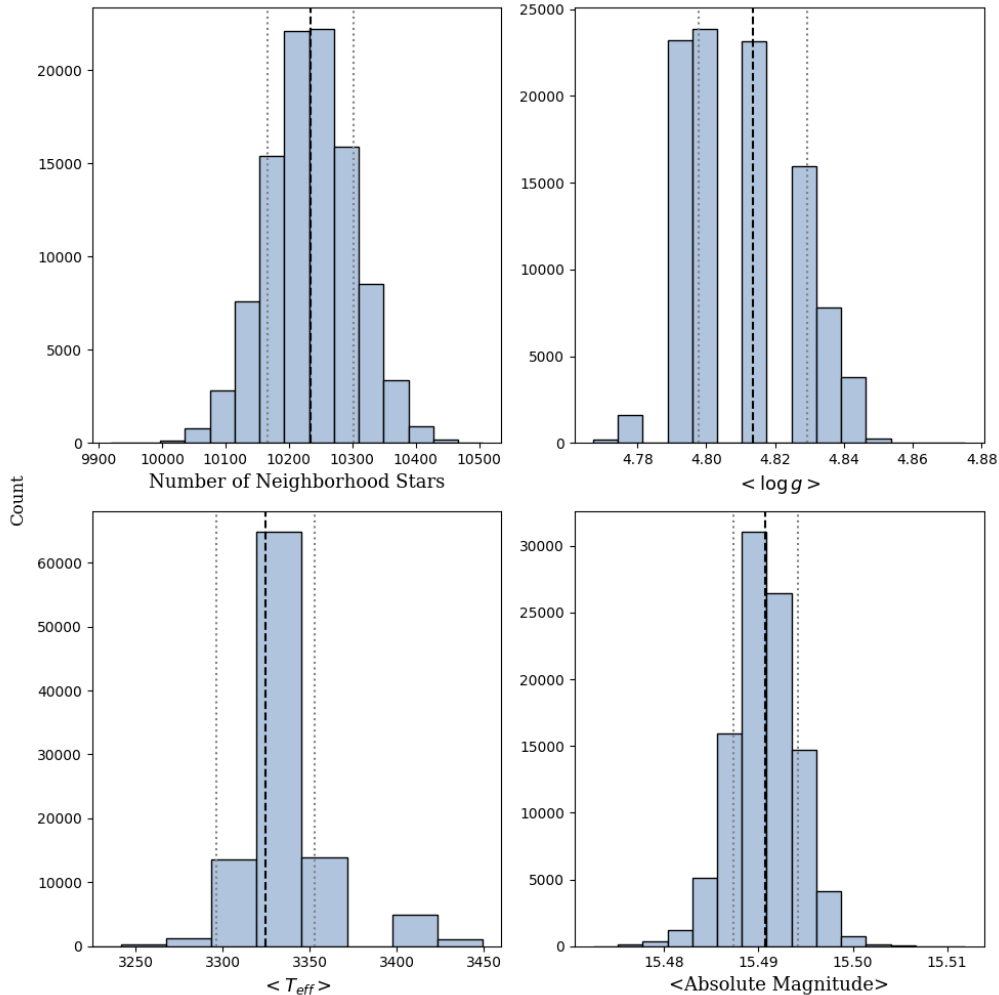


**Figure 15.** Bootstrapped sampling distributions of neighborhood star count (top-left panel) and astrophysical parameters:  $\langle \log g \rangle$  (top-right panel),  $\langle T_{\text{eff}} \rangle$  (bottom-left panel) and  $\langle \text{Absolute Magnitude} \rangle$  (bottom-right panel) of the 10 pc environment of HD 165155. Gray dotted lines represent the standard deviation and the black dashed lines represent the median.

We first confirmed that all three high-density HZS are indeed located near the galactic plane (see Figure 1), where the background star density is particularly high. In addition to HD 165155, HD 159868, and HD 188015, there are five other HZS located in the foreground of the high-density region of the galactic plane, though their 10 pc volume does not differ significantly from that of the Sun. This dissimilarity implies that the neighborhood data compiled from Gaia DR3 is highly accurate and reliable, even for HZS located near the galactic plane.

We also find that the distance between HD 165155 and HD 159868 is 16.5 pc, indicating that both systems are embedded in a similar stellar environment. In contrast, HD 188015 is about 60 pc away from these systems and roughly 50 pc from the Sun, which happens to be a relatively less dense environment.

Rybizki et al. (2022), developed a classifier for Gaia eDR3 sources to identify astrometric solutions as either **good** or **bad**. They set the `parallax_over_error` threshold  $>4.5$  for high signal-to-noise ratio regimes. In our data  $\sim 99\%$  of the sources within the 10 pc neighborhood of these high-density regions fall in that regime. Moreover, their analysis indicates that at a threshold of `parallax_over_error`  $>10$ , the number of **bad** sources is  $<10\%$ . This serves as a strong constraint for good astrometric sources.

As an additional and independent test, we also employed Monte Carlo simulations to estimate the statistical likelihood of observing high stellar density regions within the 100 pc solar neighborhood. To this end, a raw sample of  $\sim 570,000$  stars was compiled by selecting all stellar sources with a Gaia-measured parallax of  $\geq 10$  mas. From this 100 pc sample, we randomly selected points in RA [0,360], Dec [-90,90], and parallax [11.11,1000] mas, and for each point, we counted

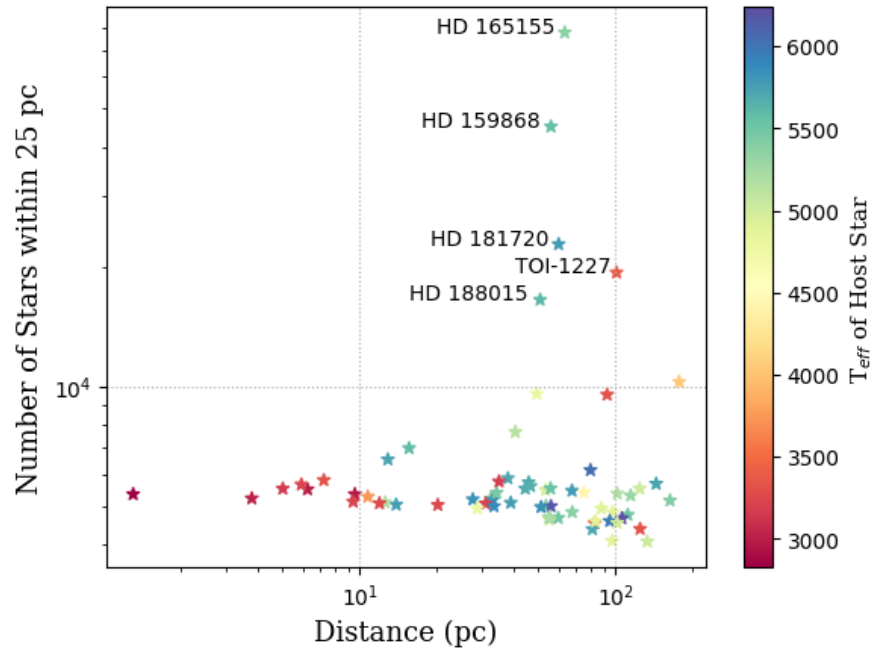


**Figure 16.** The 25 pc neighborhood star count for 84 HZS and their distance from Sun. The colorbar represents the effective temperature  $T_{\text{eff}}$  (K) of HZ stars. The names of 5 HZS with highest star count are also labeled.

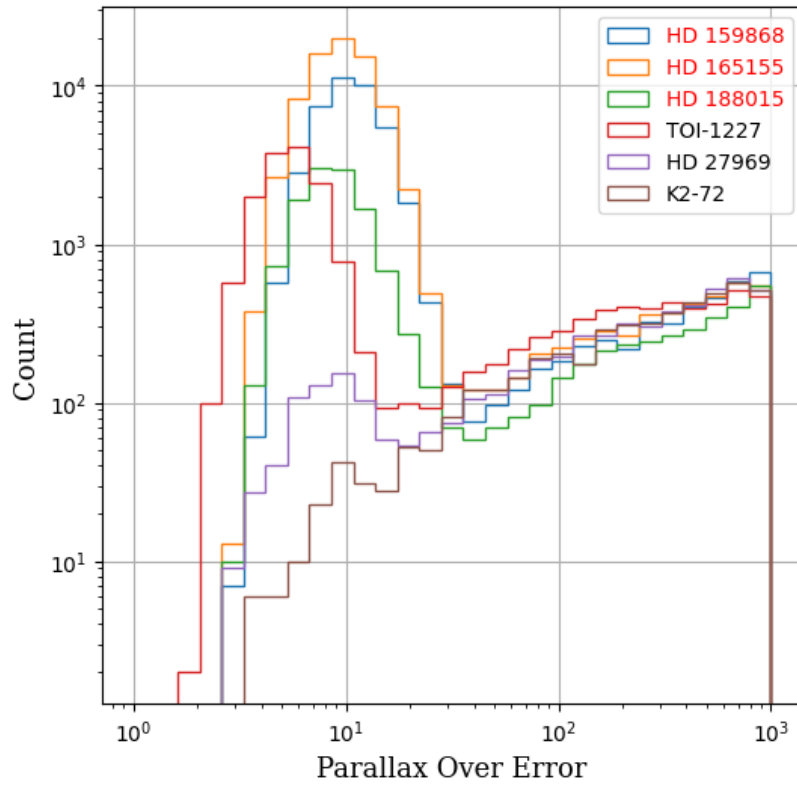


**Figure 17.** Distribution of `parallax_over_error` for stars in 25 pc neighborhood around 6 HZS. The names of 3 HZS with the highest star count in their 10 pc regions are indicated in the legend with red.

the number of stars within its 10 pc neighborhood. This process was repeated one million times. We found that the probability of obtaining  $>10,000$  stars in 10 pc volume around random locations is 0.14% and that of obtaining  $>2000$  is 1.7%. These results suggest that while the neighborhoods of the three HZS in question seem rare, occurrence of dense regions of stars within 100 pc of Sun is not entirely improbable.

Finally, we plot the 25 pc neighborhood star count for the 84 HZS in Figure 16. Similar to the 10 pc region, the 25 pc star count around HD 165155 remains highest ( $\sim 77,000$ ), followed by  $\sim 45,000$  stars around HD 159868. However, the 15-fold increase in volume resulted in less than an 8-fold increase in star count, indicating a notable density drop in going from 10 pc to 25 pc region. We would not expect such a drop if the background stars near the galactic plane were contaminating the neighborhood sample.

Figure 17 represents the distribution of the `parallax_over_error` for sources within the 25 pc radius of 3 HZS that have the highest population within their 10 pc radius and 3 HZS that have a lower population ( $<1000$ ) in their 10 pc neighborhood. This plot indicates that most environments have a majority of sources with high signal to noise ratio (`parallax_over_error`  $\gtrsim 10$ ) and hence have good astrometric solutions (Rybizki et al. 2022). The sharp decline on the left slope also suggests the presence of a smaller number of high parallax error sources. A value  $\geq 10$  indicates that the parallax error does not result in a distance error  $\geq 10$  pc for any source within 100 pc. The closer the object, the lesser is the error in distance. In conclusion, although our neighborhood sample may not be entirely free from spurious sources, the robust astrometric solutions from Gaia, combined with our bootstrap approach, provide a reliable method for studying the neighborhood demographics of HZS.